AD-A185 931 MIDDLE ATMOSPHERIC WIND MEASUREMENTS USING A MEDIUM FREQUENCY RADAR(U) AIR FORCE INST OF TECH WRIGHT-PATTERSON AFB OH B B COBLE 1987 1/1

UNCLASSIFIED AFIT/CI/NR-87-123T F/G 17/9 NL

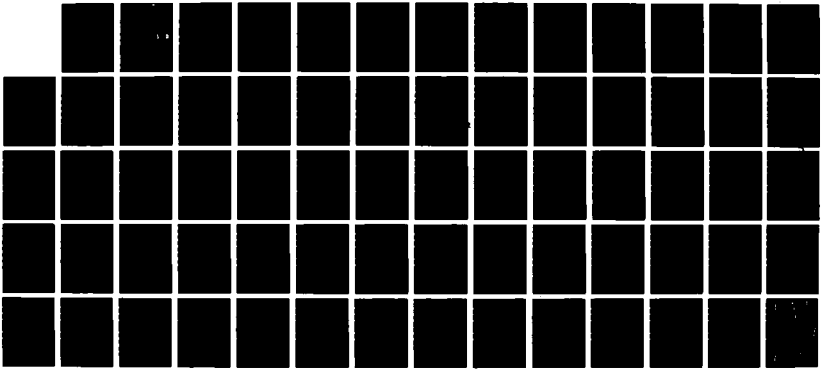

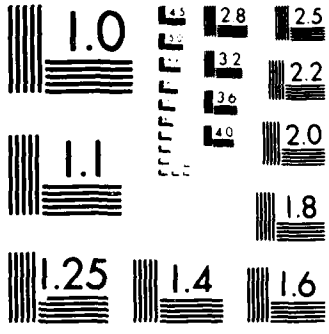

SECURITY CLASSIFICATION OF THIS PAGE (When Data Entered)

REPORT DOCUMENTATION PAGE

READ INSTRUCTIONS BEFORE COMPLETING FORM

1. REPORT NUMBER: AFIT/CI/NR 87- ~~087~~ 123T	2. GOVT ACCESSION NO. / 3. RECIPIENT'S CATALOG NUMBER
4. TITLE (and Subtitle): Middle Atmospheric Wind Measurements Using A Medium Frequency Radar	5. TYPE OF REPORT & PERIOD COVERED: THESIS/DISSERTATION
	6. PERFORMING ORG. REPORT NUMBER
7. AUTHOR(s): Barry Byron Coble	8. CONTRACT OR GRANT NUMBER(s)
9. PERFORMING ORGANIZATION NAME AND ADDRESS: AFIT STUDENT AT: Utah State University	10. PROGRAM ELEMENT, PROJECT, TASK AREA & WORK UNIT NUMBERS
11. CONTROLLING OFFICE NAME AND ADDRESS: AFIT/NR WPAFB OH 45433-6583	12. REPORT DATE: 1987
	13. NUMBER OF PAGES: 58
14. MONITORING AGENCY NAME & ADDRESS (if different from Controlling Office)	15. SECURITY CLASS. (of this report): UNCLASSIFIED
	15a. DECLASSIFICATION/DOWNGRADING SCHEDULE

16. DISTRIBUTION STATEMENT (of this Report)

APPROVED FOR PUBLIC RELEASE; DISTRIBUTION UNLIMITED

17. DISTRIBUTION STATEMENT (of the abstract entered in Block 20, if different from Report)

18. SUPPLEMENTARY NOTES

APPROVED FOR PUBLIC RELEASE: IAW AFR 190-1

LYNN E. WOLAVER 22 Sep 87
Dean for Research and Professional Development
AFIT/NR

19. KEY WORDS (Continue on reverse side if necessary and identify by block number)

20. ABSTRACT (Continue on reverse side if necessary and identify by block number)

ATTACHED

DD FORM 1 JAN 73 1473 EDITION OF 1 NOV 65 IS OBSOLETE

SECURITY CLASSIFICATION OF THIS PAGE (When Data Entered)

MIDDLE ATMOSPHERIC WIND MEASUREMENTS

USING A MEDIUM FREQUENCY RADAR

by

Barry Byron Coble

A thesis submitted in partial fulfillment

of the requirements for the degree

of

MASTER OF SCIENCE

in

Soil Science and Biometeorology

Approved:

Gene W Adams
Major Professor

Committee Member

Lawrence E. Hipps
Committee Member

Lawrence A. Pettit
Dean of Graduate Studies

UTAH STATE UNIVERSITY

Logan, Utah

1987

ACKNOWLEDGEMENTS

The data acquisition and analysis was supported by the National Science Foundation under grants ATM-8117275, ATM-8419810, and ATM-8608391. It was also sponsored in part by the Air Force Geophysical Laboratory under contract F19628-83-C-0056 as part of the MAPSTAR project, and by a grant from IDI, Inc. This research was conducted under the supervision of Dr. Gene W. Adams of the Center for Atmospheric and Space Sciences at Utah State University. I would like to take this opportunity to express my thanks to him for his excellent guidance and friendship during this endeavor.

I would also like to express my sincere appreciation to Dr. Larry H. Hipps and Dr. L. Rex Megill of my Graduate Committee for their guidance and help with this thesis; Mr. John W. Brosnahan of Tycho Technology, Inc., for his insights concerning the construction of the radar itself; Reese Johnson and Dave Otteson, undergraduate students involved in developing a majority of the software used for the analysis; and the National Climatic Center in Asheville, North Carolina, for their timely response to my request for data.

I also want to thank the United States Air Force and the Air Force Institute of Technology for affording me this

opportunity to further pursue my education. As always, I continue to AIM HIGH!

Barry Byron Coble

TABLE OF CONTENTS

LIST OF FIGURES

Figure Page

ABSTRACT

Middle Atmospheric Wind Measurements
Using a Medium Frequency Radar

by

Barry Byron Coble, Master of Science
Utah State University, 1987

Major Professor: Dr. Gene W. Adams
Department: Soil Science and Biometeorology

The Imaging Middle-Atmospheric Geophysical Radar was located at the Boot Lake, Colorado, field site and operated at 2.66 megahertz to collect radar data. The data presented here were collected from 2120 Universal Time to 2310 Universal Time on March 20, 1983. It was operated as a Doppler interferometer to measure winds in the middle atmosphere (16.5 - 91.5 kilometers), which includes the stratosphere and the mesosphere. Highly specular returns were obtained in the lower regions of the middle atmosphere, with specularity increasing as altitude decreased. Algorithms were developed to take these specular returns and derive useful wind speeds and directions in a region of the middle atmosphere, 30 - 55 kilometers, which had not previously yielded such information easily. Three-dimensional wind vectors were derived, and these values agreed well in

direction, but overstated the magnitude when compared with rawinsonde data in the 16.5 - 30 kilometers region. The rawinsonde data were taken at Denver, Colorado, at time periods before and after the data run.

(58 pages)

CHAPTER I

INTRODUCTION

There exist today several techniques with which to study the region between 10 Km and 100 Km, known as the middle atmosphere. These techniques are rather recent in development, and are indicative of Man's advancements in the fields of science and engineering. As with many other achievements of Man, however, these techniques do have their problems and limitations.

The measurement of wind velocities in the middle atmosphere has been the prime focus of many techniques. These range from the use of radio-theodolite tracked balloons to the tracking of satellites high above the surface of the earth. Included in these techniques is the use of radar in detecting winds in the middle atmosphere. Radar has become one of the more promising techniques to be used to measure the middle atmosphere due to its relatively low cost of operation and its capability of providing real-time continuous data.

There are a variety of techniques which can provide data on a variety of atmospheric parameters of the middle atmosphere. These include the mesosphere-stratosphere-troposphere (MST) radar, the spaced antenna drift (SAD) radar, the incoherent scatter radar, and the meteor radar.

All types have provided excellent results in obtaining wind velocity measurements for certain regions of the atmosphere. See Figure 1 for a graphic representation of the various measurement techniques for the Middle Atmosphere (as cited in Gage and VanZandt, 1981).

None of these methods, though, have provided very good results for a critical region of the middle atmosphere from 30 Km to 60 Km. This is due primarily to the type of scattering being measured by the particular radar. As is apparent in the name, the meteor radar detects the ionized trail left by a meteor as it disintegrates in the atmosphere above 80 Km. This height limitation precludes this radar from providing data in the 30 - 60 Km range. The incoherent scatter radar gets useful returns only from the mesosphere and above (i.e., above 60 Km). Both the MST and SAD techniques can detect scattering in the troposphere and lower stratosphere as well as in the mesosphere. But neither technique is powerful enough to detect returns from the critical region (Larsen, 1983).

This is not to say that the MST and SAD techniques have not detected returns in the critical region. The returns detected, however have been so weak and sparse that it would take long integration times (30 minutes or more) to provide enough data to make wind velocity determinations. At these long integration times the measurements are likely to be contaminated by the presence of long period wave structures, such as gravity waves (Royrvik, 1983).

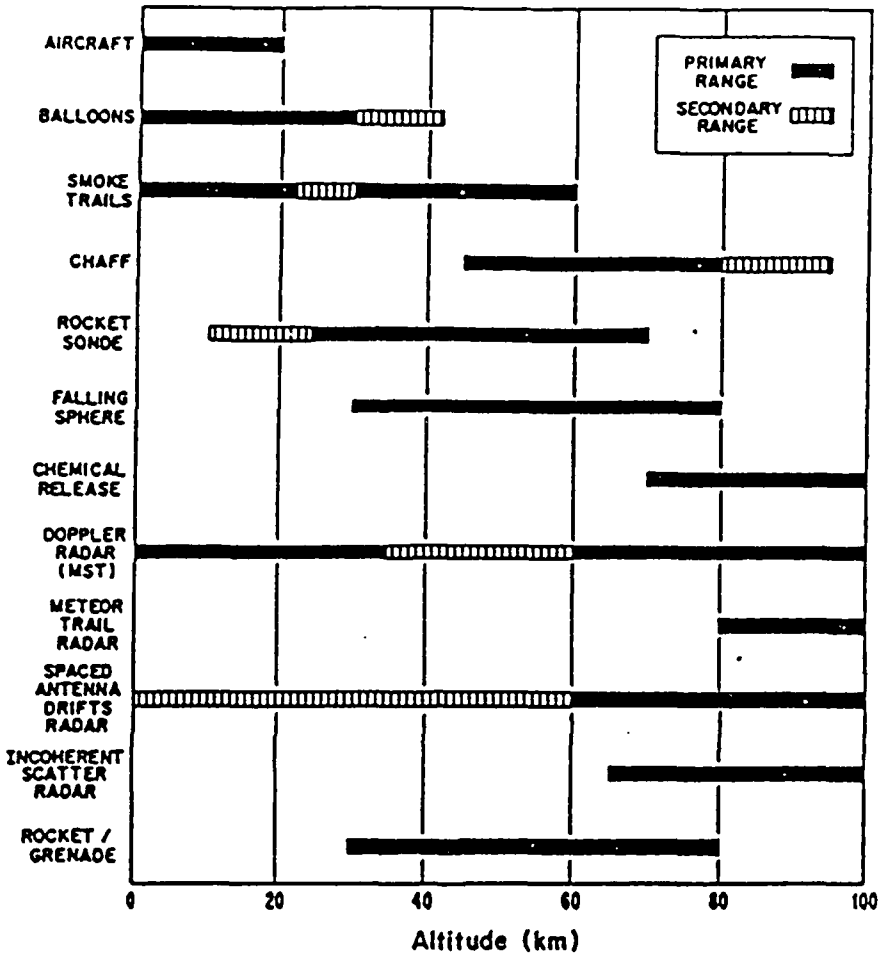

Fig. 1. Various middle atmospheric measurement techniques.

A new radar technique has been developed which can possibly overcome some of the shortcomings of the previously mentioned techniques (Adams et al., 1986). The use of Doppler interferometry may make it possible to determine winds for the entire middle atmospheric range. Briefly, the technique is able to view a large volume simultaneously and determine the locations of a number of Doppler-spectral features, or scattering points. From the Doppler shifts and locations of the spectral features, a wind speed and direction may be determined for the volume of air illuminated at each altitude. This technique is more sensitive than other radar techniques, which may make it possible to determine winds in the critical region.

The objectives of this thesis are as follows:

1) Determine the wind from the scattering points returned by the radar using software developed for this purpose. This software is discussed in both the literature review and data analysis sections of this thesis.

2) If winds can be determined, compare the results at the lowest altitude with results obtained from existing nearby ST radar and/or rawinsonde data from nearby reporting stations.

3) If winds cannot be determined through the entire altitude range, show the bottom and top altitude limits, speculate as to why the technique

fails, and propose techniques that could be used to make it feasible.

CHAPTER II

LITERATURE REVIEW

Probing of the atmosphere by a radar depends on the scattering and reflection from spatial refractive index variations. Depending on the altitude being considered, these variations can correspond to any change in pressure, humidity, temperature or electron density. It is these changes that cause the electromagnetic waves of a radar signal to be scattered or reflected (Rottger, 1980).

These changes in the refractive index can best be illustrated as follows. The radio index of refraction is given approximately by the following formula (as cited in Balsley and Gage, 1980):

$$n - 1 = (3.73 \times 10^{-1} e)/T^2 + (7.76 \times 10^{-6} P)/T - N_e/2N_c$$

where n = the refractive index, P = the atmospheric pressure in millibars, e = the partial pressure of water vapor in millibars, T = the absolute temperature, N_e = the number density of electrons, and $N_c = 1.24 \times 10^{-2} f^2$ where f = the critical frequency in MHz and, therefore, N_c = the critical plasma density in MKS units. The first term on the right hand side refers to the contributions to refractive index changes made by fluctuations in the density of water vapor. This term is only important in the lower

troposphere where water vapor is abundant. The second term on the right hand refers to density fluctuations in dry air. This term is most important from the upper troposphere to the stratopause. The third term on the right hand side refers to refractive index changes caused by the presence of free electrons. It becomes an important factor above the stratopause (≈50Km) where electron density increase rapidly with height.

Evaluating the above equation reveals that the first term is of no consequence when dealing with the atmosphere above 15 Km. Below 50 Km the second term of the equation dominates, while above 50 Km the third term dominates. The region between 15 and 50 Km in altitude provides the smallest refractive index change. This is due to decreasing atmospheric density and the lack of free electrons below the stratopause. This can best be illustrated by Figure 2, which shows how the power returned by scattering points falls off to a minimum near 50 Km.

These variations may be caused mainly by turbulent fluctuations yielding partial (Fresnel) refractions from coherent discontinuities in the troposphere and stratosphere. Radar signals can also be scattered back from ionospheric structures in the mesosphere and thermosphere. Because of strong collisional coupling between ionized and neutral particles in this region of the atmosphere, the level of scattering is an excellent indication of neutral

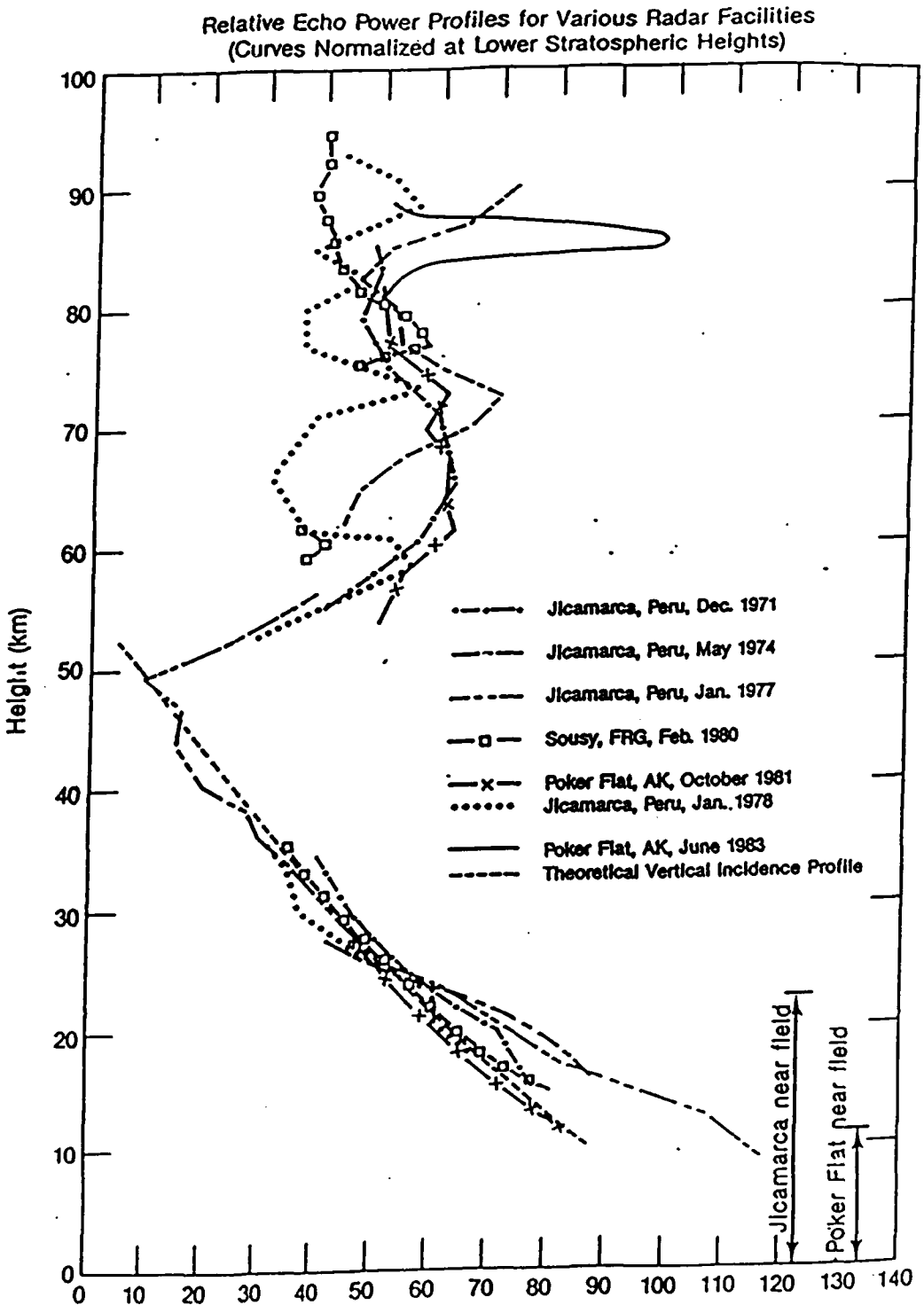

Fig. 2. Relative power profiles for several radar facilities around the world.

atmospheric dynamics in the middle atmosphere (Rottger, 1981; Balsley and Gage, 1981).

Reflections in the stratosphere due to the presence of thin stratified layers can enhance the amount of power returned. It is here that the use of the term aspect sensitivity comes into focus. Aspect sensitivity can be defined as the property of a scattering point to have a higher power return as it approaches the zero zenith angle of the radar beam, i.e., to behave like a mirror. If one refers to the divisions of the atmosphere as defined by the temperature profile, aspect sensitivity has been reported to increase with decreasing altitude to a maximum near the tropopause (Tsuda et al., 1986). It is also present throughout the middle atmosphere, which is illustrated in Figure 3 for the stratosphere and in Figure 4 for the mesosphere. These figures show how, with decreasing altitude, the amount of power returned to the radar increase toward a maximum value near the zero zenith angle. These figures also illustrate the fact that aspect sensitivity reaches a maximum near the tropopause (Johnson et al., 1986). Aspect sensitivity has, for years, been considered a bane to radar detection since the higher power return near the zenith tends to dominate what might otherwise be valid radar returns from off zenith angles (Tsuda et al., 1986).

The Doppler interferometer method, however, coupled with appropriate software for data analysis, could possibly use the data received from scattering points exhibiting

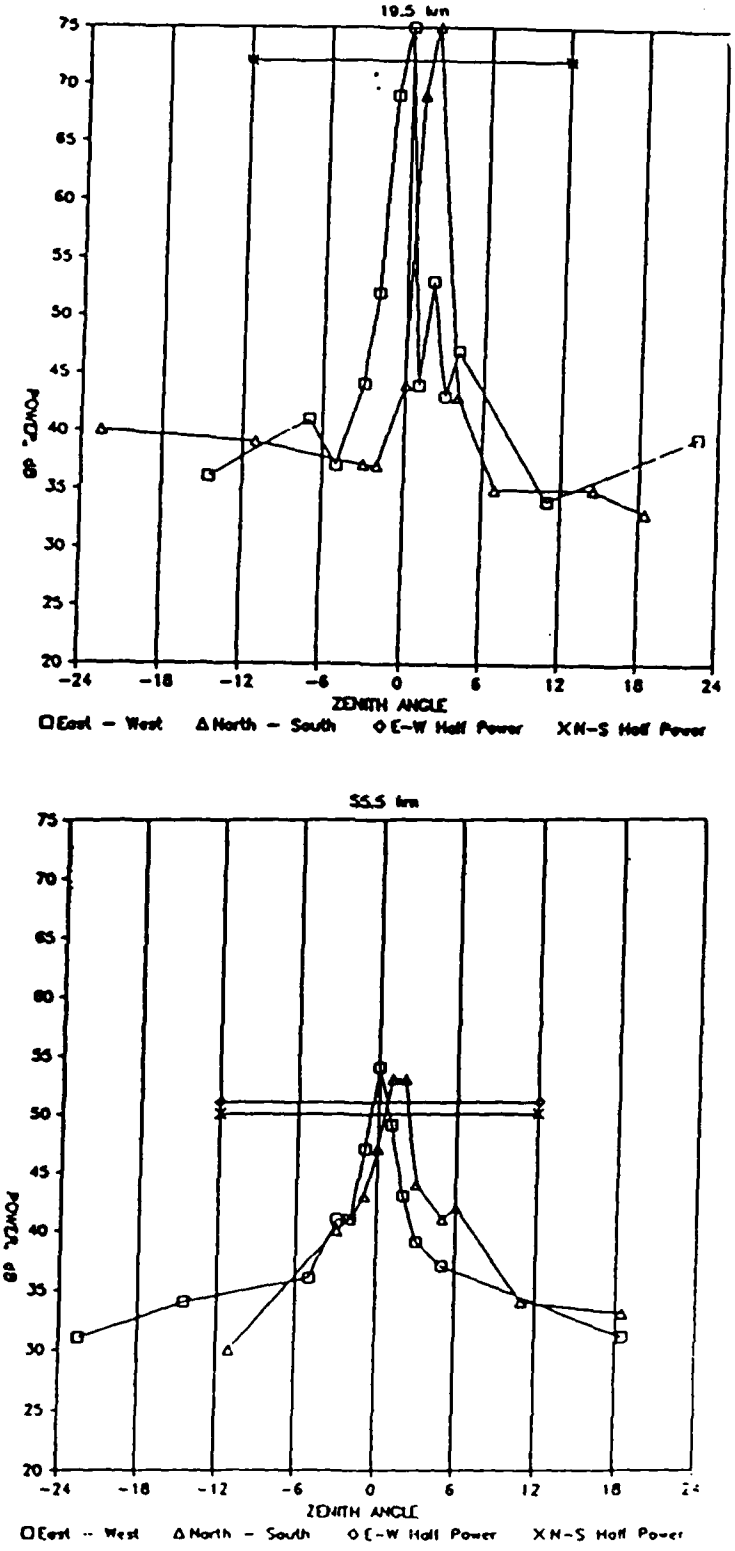

Fig. 3. Aspect sensitivity profiles from 19.5 Km to 55.5 Km.

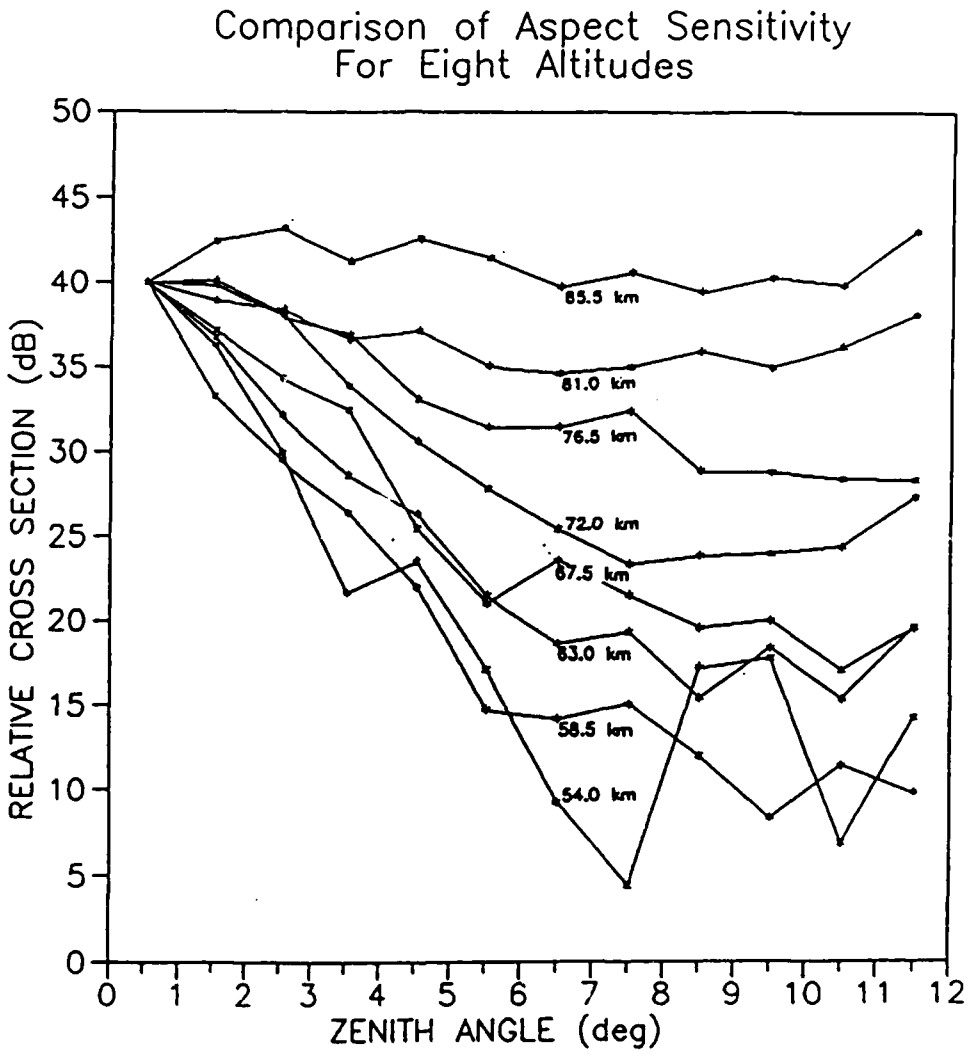

Fig. 4. Comparison of aspect sensitivity in the mesosphere.

aspect sensitivity, or specularity. Since these points are a result of turbulent fluctuations of stratified layers, it only becomes a matter of utilizing a method which is sensitive enough to successfully separate these points from false echoes. The Doppler interferometer method provides much better spatial resolution than other methods and, thus, can much more easily separate points near the vertical (zero) zenith angle. Above the stratopause aspect sensitivity is itself overwhelmed by the rising isotropic component of returns (Adams et al., 1986).

The radar interferometry method can be defined as making use of phase differences between signals received at two or more spatial locations. At the frequency of 2.66 MHz it is possible to measure the phases of the received voltages on two or more antennas simultaneously. These phase differences occur between those voltages received from the parallel antennas in the north-south antenna complex to get the east-west zenith angle, and similarly for the east-west antenna complex to get the north-south zenith angle.

The first attempt at using the radar interferometer technique to measure an atmospheric parameter, in this case the direction of the magnetic field at ionospheric heights, was made in 1971 by R.F. Woodman at the Jicamarca Observatory in Peru with very high accuracy in comparison with known results (Woodman, 1971). Since then it has been used

to study such subjects as plasma turbulence in the upper atmosphere, F - region irregularities, and auroral electrojet irregularities. It has only been recently, however, that true interferometer observations have been attempted below the ionosphere (Farley, 1983).

Basically, the radar interferometer technique involves two or more antennas, each with its own receiver, and a transmitting antenna or antennas. The transmitting antenna(s) can also serve as a receiving antenna(s). Suppose there is a point or target at some angle θ from the zenith in the plane defined by the vertical and a line joining the phase centers of the receiving antennas. This can be translated into a phase difference defined by:

$$\Delta \phi = k\ L\ \sin\theta$$

where $k = [2\pi / \lambda]$, the radar wave number and L = the separation of the antennas. Figure 5 shows this setup graphically. If, however, the target is moving, then Doppler shifts in the received signals will occur. This Doppler shifting can give additional information and help separate multiple targets in the radar beam. Thus by determining the radial velocity of at least three individual targets at a certain altitude, a bulk flow velocity at that altitude can also be determined. In this case wind velocity refers to the measurement of bulk wind flow over an area of approximately 10 - 100 Km on a side in the horizontal plane (Farley, 1983).

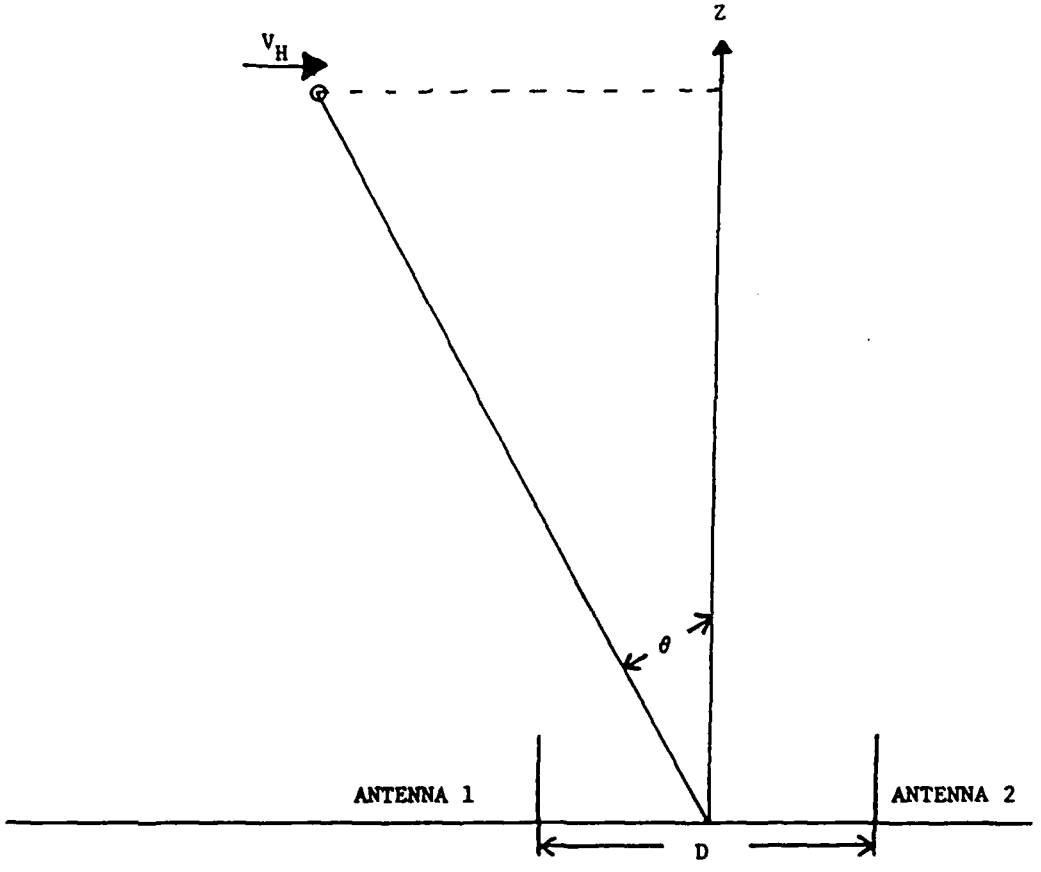

Fig. 5. Diagram of a single target as detected from two antennas.

1. Imaging Doppler interferometry

The method used to analyze the data described here, the Doppler or radar interferometry method, first involves Fourier transforming the time domain of recorded complex voltages from each antenna into the frequency domain, then using interferometry. This is a very productive method for separating multiple targets.

Figure 6 and Figure 7 show a graphic example of what is being described. Figure 6 illustrates two targets as being detected by the IMAGER, with their respective zenith angles. This is only shown for two antennas. Figure 7 shows how it is possible to measure the location and velocity of two targets by Fourier-transforming time series of the two complex voltages to get two power and phase spectra. In this figure ω_a and ω_b refer to the two targets as identified by the radar.

For each Fourier frequency or Doppler shift each antenna array is examined separately. A valid scattering point will give a constant antenna-to-antenna phase difference. Both power spectra identify the same Doppler frequency of the target f_T. Given this f_T, it is possible to achieve the radial velocity v_R as follows:

$$V_R = f_T c/2F = V_H \sin\theta$$

where F is the radar frequency and C is the speed of light. The difference in phase angle values at f_T can be used in

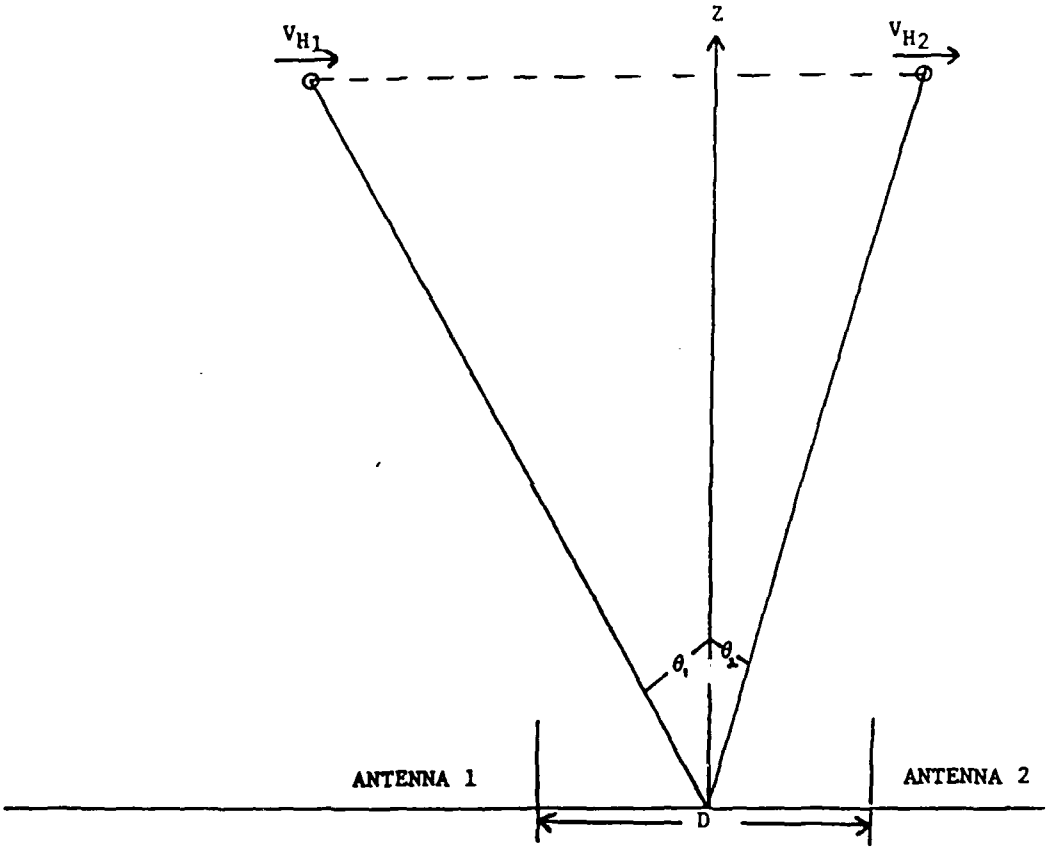

Fig. 6. Diagram of a two target configuration as observed from two antennas.

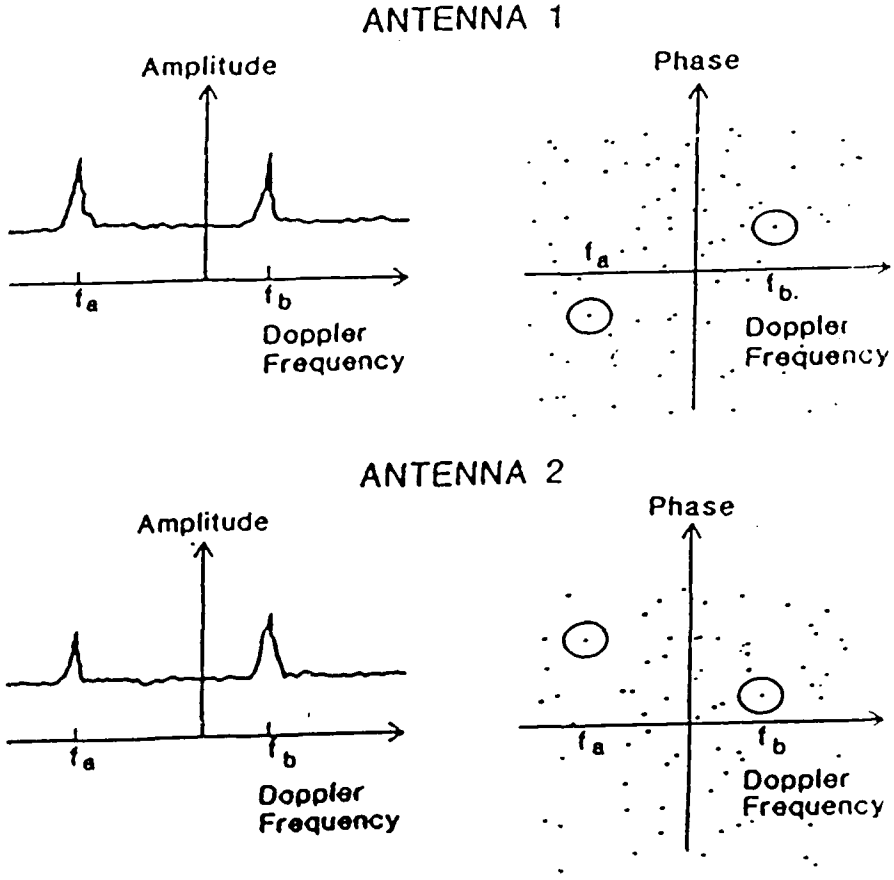

Fig. 7. Graphic depiction of observed power and phase returns from two antennas.

the following equation to calculate the zenith angle:

$$\theta = \sin^{-1} [\lambda \Delta \phi / 2 \pi L]$$

where L is the spacing in meters between the two antennas (Adams et al., 1986).

This method is adequate for just two antennas. With the IMAGER are ten antennas, so a slightly different approach is used. The data from the two antenna arrays (north-south and east-west) are processed separately. Then a least-squares straight line is fit to the five phase values vs the antenna spacing for that particular array. Each phase value is first corrected for the time lag introduced relative to the values for the two receivers in the middle of the array. Then a root mean square (rms) error of the fit of the phase values is used to decide which points are to be considered good. By accepting points whose rms errors were 30° in phase or less for both arrays, a small percentage of random points were accepted as good data points while the percentage of useful data points remained high. This rms error corresponded to a horizontal resolution of 1.35 Km at an altitude of 100 Km. As mentioned earlier, the range-gate spacing was set at 1.5 Km, but the pulse length was 4.5 Km so it can be conservatively estimated that the spatial resolution of the IMAGER was plus or minus 5 Km in each of the three spatial coordinates (Adams et al., 1986).

Now the zenith angles of the two arrays can be determined using the following formulas:

$$\theta_{NS} = \sin^{-1}(D_{ew}/4.442)$$

$$\theta_{EW} = \sin^{-1}(D_{ns}/4.442)$$

where D of the respective arrays represents the slopes of the fitted lines to the phases of those arrays.

Now the following information exists for each scattering point:

V_r = The radial velocity

R = The range gate, in 1.5 Km steps

θ_{ew} = The zenith angle in the East-West plane

θ_{ns} = The zenith angle in the North-South plane

The range R and the two zenith angles combine to form a three-dimensional coordinate system which can be translated into a Cartesian coordinate system where X is east, Y is north, and Z is vertical. It is then possible to sort the points according to altitude.

Having since determined the location of each scattering point, it is now possible to determine the vector radial velocity as:

$$\bar{V}_{Rj} = V_{Rj}\bar{1}_{Rj}$$

where j = 1, 2, 3, ..., J, where J is the number of scattering points identified at a given altitude, and 1_{Rj} is a unit

vector in the radial direction passing through the jth point, and is given by:

$$\bar{1}_{Rj} = 1_j\bar{1}_x + m_j\bar{1}_y + n_j\bar{1}_z$$

where 1_j, m_j, and n_j are the direction cosines of the jth scattering point, given by:

$$1 = \sin \theta_{EW}$$

$$m = \sin \theta_{NS}$$

$$n = (1 - 1^2 - m^2)^{1/2}$$

From this, then, the mean apparent motion vector can be given by:

$$\bar{V}_m = u\bar{1}_x + v\bar{1}_y + w\bar{1}_z$$

Three scattering points are sufficient to determine the three components of the motion. With more than three points it is possible to calculate a least-squares fit to the scattering-point parameters as follows: Since

$$\bar{V}_{Rj} = \bar{V}_m\bar{1}_{Rj}$$

for all j if the rms fit is perfect, the rms error is given by:

$$\epsilon = (1/J)[V_R-(ul_j + wn_j)]^2)^{1/2}$$

In order to minimize the rms error, the following is required:

$$\partial \epsilon / \partial u = \partial \epsilon / \partial v = \partial \epsilon / \partial w = 0$$

which gives

$$u\sum l_j^2 + v\sum l_j m_j + w\sum l_j n_j = \sum V_{Rj} l_j$$
$$u\sum l_j m_j + v\sum m_j^2 + w\sum m_j n_j = \sum V_{Rj} m_j$$
$$u\sum l_j n_j + v\sum m_j n_j + w\sum n_j^2 = \sum V_{Rj} n_j$$

These are then solved for u, v, and w.

The number of valid scattering points can be affected by the amount of noise present in the data. This noise can be caused by transmitter ringing, by cosmic noise sources not at 2.66 MHz such as the sun, by the presence of thunderstorms near the radar, and by man-made noise sources near the radar (TV or radio transmissions, generators, etc.). In addition, Stubbs (1973) points out that noise is more of a problem at night. Noise can often be filtered out of the data or removed via coherent averaging (Vincent, 1984).

CHAPTER III

DATA ANALYSIS

A majority of the following information is taken from two articles written by Dr. Gene W. Adams (Adams et al., 1985, and Adams et al., 1986).

1. The IMAGER

The data used for the analysis were collected via the Imaging Middle-Atmospheric Geophysical Radar (IMAGER), which was located at the Boot Lake field site 10 miles east of Brighton, Colorado. The IMAGER was operated at a frequency of 2.66 MHz with 50 kW peak-pulse-power in 30-μs Gaussian pulses. Ten independent coaxial-collinear antennas were used; five were parallel and ran east-west, and the other five were parallel and ran north-south. Figure 8 depicts graphically how the radar was set up. Each antenna consisted of 8 half-wave dipoles connected end-to-end with a 180-degree phase reversal at each junction. This gave it the appearance of a length of coaxial cable with periodic splices. All ten antennas were used simultaneously for transmission and were sampled in pairs in rapid sequence for reception. All the antennas were referenced spatially by means of a phase shift to the center pair of antennas. The longitudinal and transverse spacings of the antennas were

IMAGER (Imaging Middle - Atmosphere Geophysical Radar) ANTENNA

LOCATION: BOOT LAKE (BRIGHTON) COLORADO
AREA: 25.6 ACRES = 10^5 M^2
HEIGHT: 0.15 λ
FREQUENCY: 2.66 MHz
λ: 112.5 M

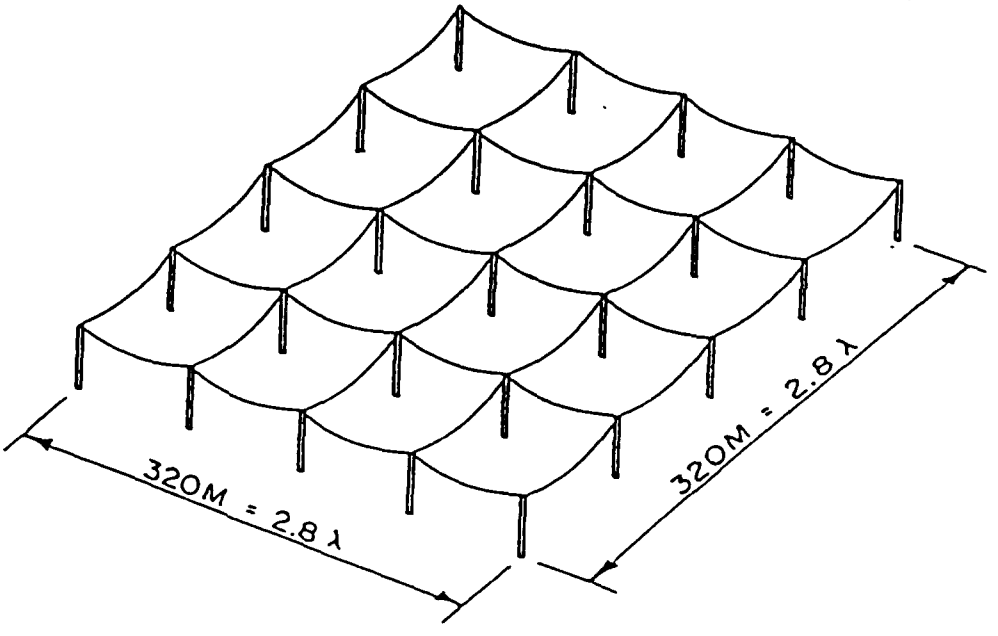

Fig. 8. The IMAGER setup.

0.33 λ and 0.707 λ , respectively, which correspond to lengths of 37m and 80m, respectively. Ten separate transmit/receive switches were used, and the transmit beam was 28° wide when all ten antennas were used.

Transmission took place at 50 pulses/sec, with a four-pulse coherent integration at each antenna pair before recording the data and moving to the next antenna pair. What are actually recorded are the complex voltages in the form of x and y voltages returned by the atmosphere, and these values are what are written to a magnetic tape before the next antenna pair is sampled. Each complete frame of data requires 0.4 seconds.

The analyzed data were recorded from 2120 UT (1420 MST) to 2310 UT (1610 MST) on March 20, 1983. The data was placed in 55 files with each file covering two minutes of data. Each file consisted of 200 pulse sets which were zero-filled to 256 pulse sets in order to use conventional FFT computer routines. Fifty range gates were used to divide the data, with each range gate spaced at 1.5 Km. The bottom altitude was at 16.5 Km, which corresponded to range 1. The top altitude was 91.5 Km (range 50).

With the antenna spacing of 0.707λ, grating lobes are formed at angles of ±45° to the zenith. That is, all scattering points that lie within 45° of the horizontal will be aliased into zenith angles of 24.5° - 45°. Therefore, all scattering points beyond the 24.5° zenith angle are located only with an ambiguity. In this experiment only

those points within 24° of the zero zenith angle are being considered (Adams et al., 1986).

2. Stratospheric wind analysis

The previously described techniques have been proven to work with returns from the mesosphere (Adams et al., 1986). However, several problems occur when attempting to utilize these techniques from the stratopause down, or from approximately 55 Km and below. As was previously stated, aspect sensitivity increases with a decrease in altitude. Figure 3 shows several plots of aspect sensitivity with increasing altitude. These plots were taken from another data set provided by the IMAGER.

Radars that are less sensitive than the IMAGER would have difficulty distinguishing between the individual scattering points found in the radar beam. Aspect sensitivity causes those points which are one on top of another in the radar beam to appear as one point with their respective power returns added together. Therefore, a single point appears to be detected with an abnormally high power return and is given too much importance when computing winds. This fact is one of the main reasons radars in the past have been unable to determine winds in this region; they have been unable to determine "real" data from "imaginary" data."

Attempts were made to avoid using data displaying aspect sensitivity. This involved eliminating those returns

within a certain number of degrees of the zero zenith angle. However, this eliminated a majority of the valid scattering points and left few, if any, valid points with which to work. As was shown in Figure 2, a majority of the power returned from these altitudes comes from near the zero zenith angle, and those returns outside of this region do not have enough power returned to be a significant factor in wind calculations.

It becomes apparent, then, that aspect sensitivity is the problem to work around. However, it has also proven to be the solution. After all, Figure 2 does show that there are returns from the critical region. It then becomes a matter of distinguishing, or separating these returns. The IMAGER proved to be sensitive enough to do just that.

Dr. Adams (Personal communication, November 1986 through January 1987) developed a scheme with which to separate individual returns. This involved dividing the volume being illuminated by the radar beam into a grid system. The volume was first divided by altitude; the volume below 57 Km and the volume above 57 Km. This was to control the size of the grid and the individual cells, or grid squares, themselves. Interactive software was developed to allow the user to vary the size of the grid and the cells. The points within a particular cell are averaged into one point in the center of that cell. Then,

using the equations on page 20, the wind calculations were made with the points determined from gridding.

Another piece of software was developed to "string" together several data files in order to provide more points with which to work. It was found through trial and error that the optimum time average of data involved putting together five files, which accounted for ten minutes worth of data. However, certain files contained so many returns that only three were needed to provide wind measurements.

CHAPTER IV

RESULTS AND DISCUSSION

The next several pages show some of the findings obtained from the IMAGER using the software developed for the data analysis. It should be noted that when this paper refers to wind velocity, it is not referring to an instantaneous velocity but a bulk flow rate. In other words, if one were to take an anemometer up to the altitudes being considered, the results obtained would not be the same as the results returned by the IMAGER. The IMAGER is averaging over an area, for example, of a horizontal plane of 1.7 Km on a side at 16.5 Km in altitude with a 6° x 6° grid system as described in the previous section. It then provides a two-dimensional cross-section of each concerned altitude and groups them together, much like a stack of playing cards. From each two-dimensional representation a bulk flow speed and direction are obtained.

It was found through trial and error that a minimum of three data files were needed before a complete horizontal wind profile from 16.5 Km to 87 Km emerged. This was equivalent to six consecutive minutes of data. This, however, was not a hard and fast rule; some files were very sparse in useable data, especially near the beginning of the data acquisition time. Near the middle of the run of

data collection several files had nearly enough data on their own to provide a complete wind profile. That is, one two minute data file had enough good scattering points to provide a complete wind profile. As a rule, a minimum of five data files were needed to provide a relatively accurate wind profile. Five files, or ten minutes of data, were sufficient to eliminate perturbations caused by noise.

Figure 9 illustrates the East-West wind speed profile. As is to be expected, winds in the stratospheric ranges are light and variable, which is indicative of the stability of this particular atmospheric region. The term HIPEX-13 refers to the title of the data set obtained at this time from the IMAGER, and it can be thought of as the total 110 minute period of data.

Figure 10 shows the North-South wind speed profile. It exhibits the same characteristics of Figure 9, and is for the same period.

Both figures show the east-west and north-south components, respectively, as derived from rawinsonde data from the National Weather Service station at Denver, Colorado, for the March 20/1200Z and the March 21/0000Z rawinsonde. Notice that the radar wind measurements are higher than those winds returned by the rawinsonde. This is due in part to the fact that the rawinsonde has better resolution and accuracy than the IMAGER at low wind speeds. The IMAGER as operated here has a resolution of plus or minus

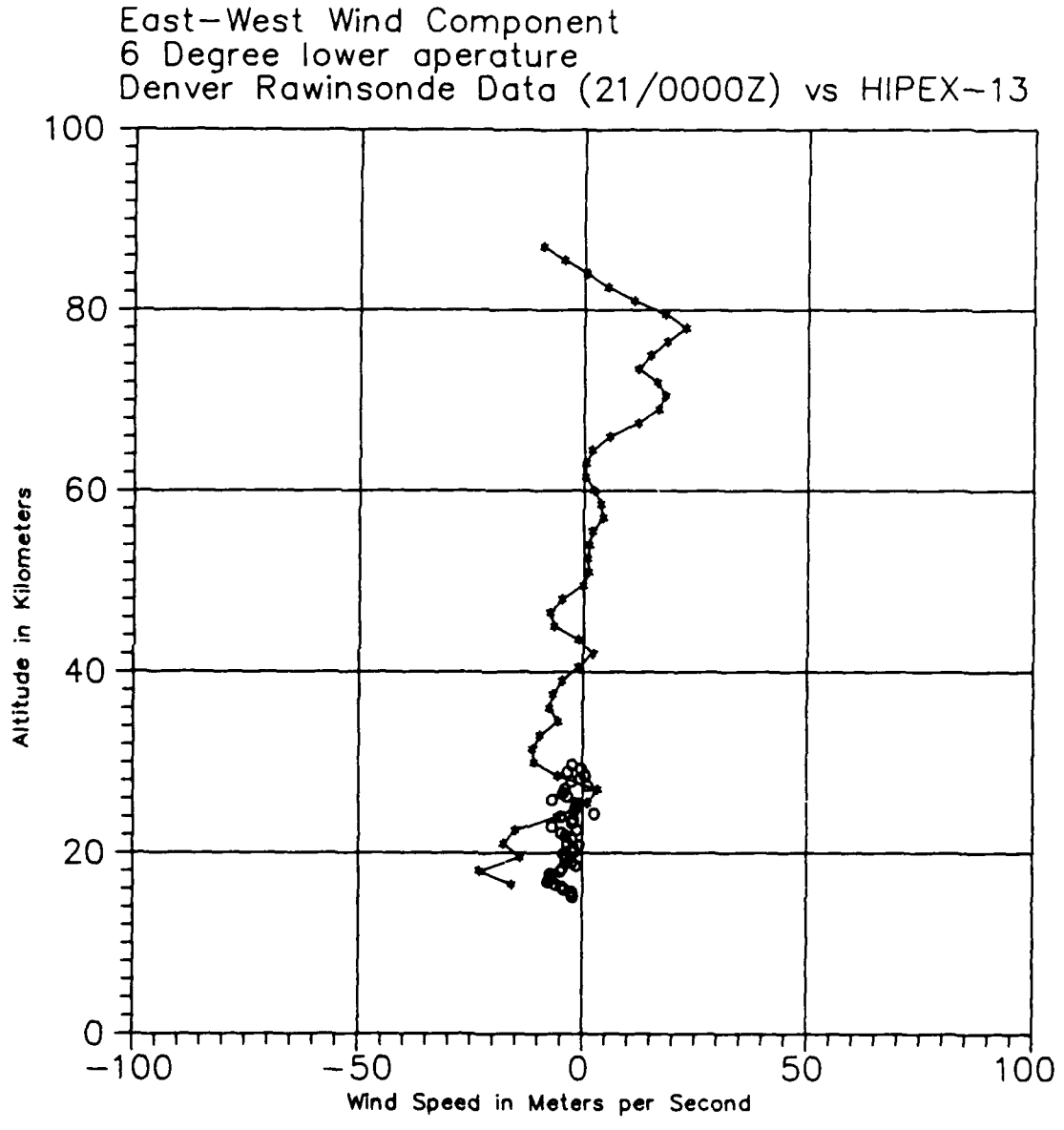

Fig. 9. A comparison of East-West wind components as returned by the IMAGER and March 21/0000Z Rawinsonde data.

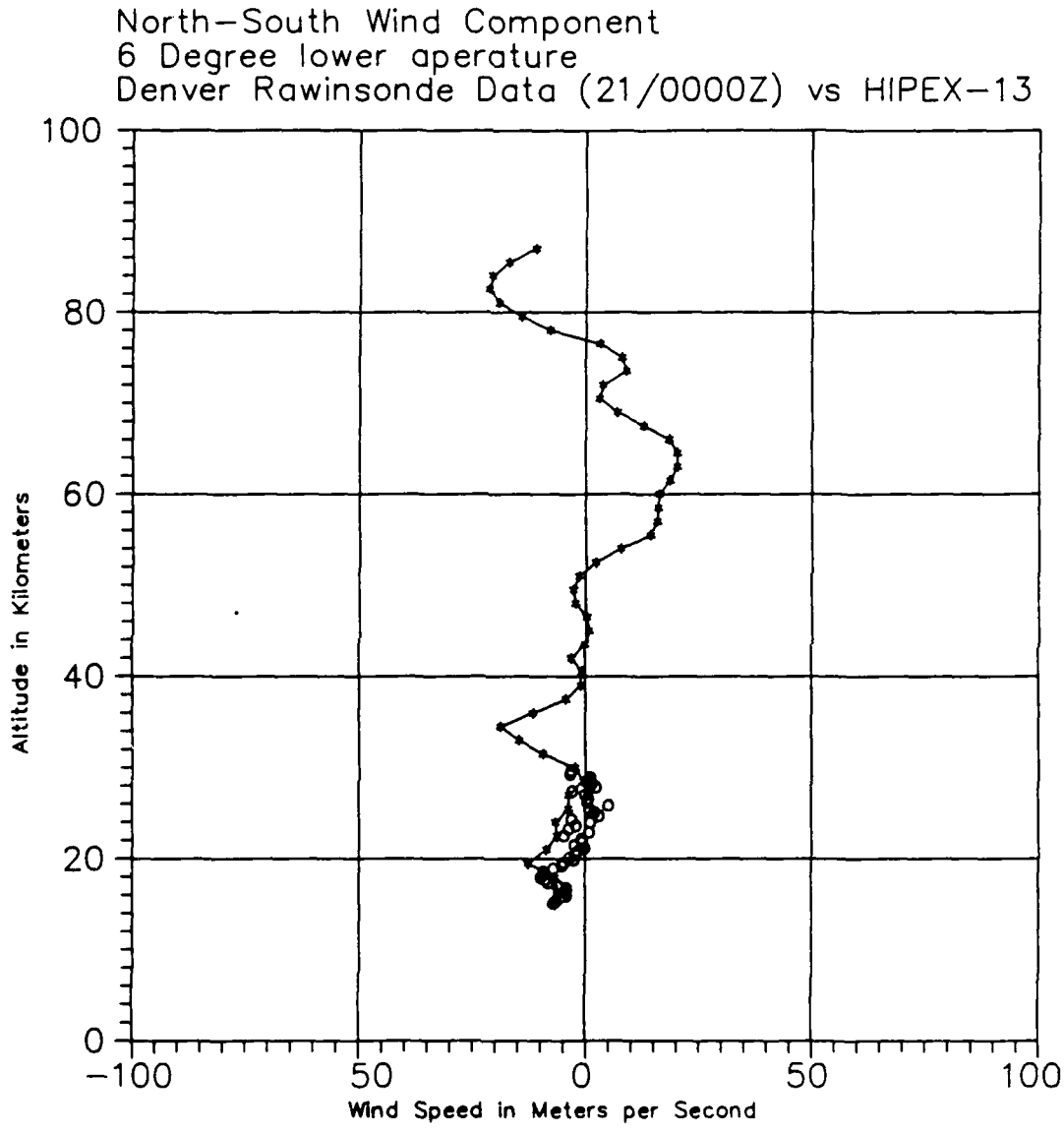

Fig. 10. A comparison of North-South wind components as returned by the IMAGER and March 21/0000Z Rawinsonde data.

10 meters per second. This is best illustrated in the following formula:

$$\text{horizontal velocity} = \pm 11.5/(N^{1/2})$$

where N is the number of scattering points used to fit the velocity. This is valid for a zenith angle of 5°, which can be considered typical. The rawinsonde can give readings down to 1 meter per second with a high degree of accuracy (Warnock et al., 1978)

Figure 11 is the horizontal wind speed profile, achieved by the following formula:

$$\text{horizontal wind speed} = \text{square root } (A^2+B^2)$$

where A is the east-west wind speed and B is the north-south wind speed. Notice how light the winds are in the region between 40 and 55 Km, and how the speed increases dramatically at the stratopause and above (55 - 60 Km). However, it must be pointed out that the software which determines the winds for the entire middle atmosphere divides the range into two separate regions with the dividing altitude at 57 Km. That is, above 57 Km the atmosphere is divided into a 24° by 24° grid system, or 12° either side of the zero zenith angle, while below 57 Km only the points within a 6° by 6° grid are used in wind calculations. Ideally, the software would allow the grid system to vary slowly as altitude increases, especially below 57 Km where the size of the grid square is critical. This again is for the

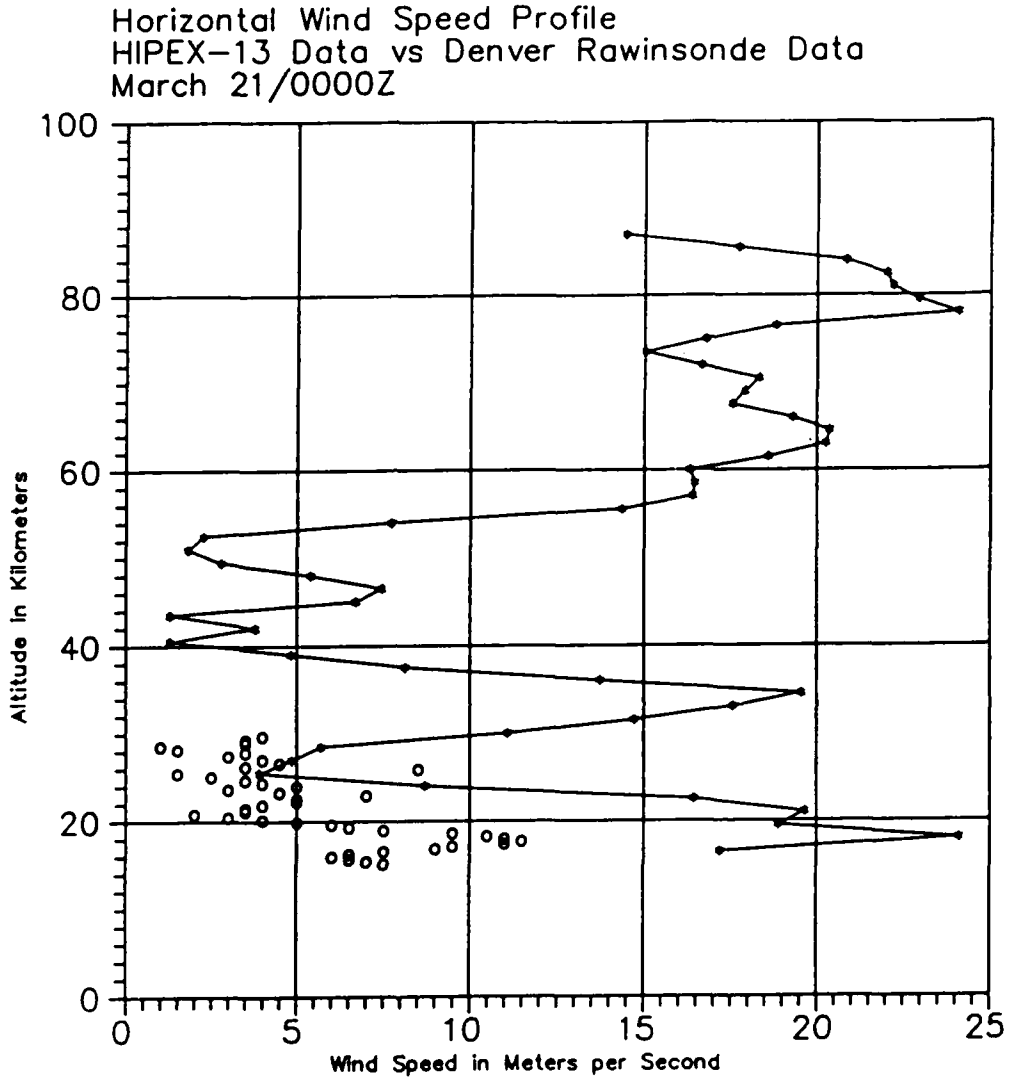

Fig. 11. A comparison of the horizontal wind speed of the IMAGER data with March 21/0000Z Rawinsonde data.

entire data set, whereas only several data files would show more variability. Near the bottom of the graph is the superimposed data as taken from the 0000Z Rawinsonde run on March 21, 1983, from Denver, Colorado.

Figure 12 illustrates the horizontal wind direction, which can be defined by the following formula:

$$\text{horizontal wind direction} = \text{TAN}^{-1}\ (B/A) - 90°$$

where B and A are the same values as defined above. Notice how the wind direction changes drastically near the stratopause. This indicates a strong shear zone, and should be investigated further to see if the IMAGER can provide such information accurately.

In Figure 13 only the altitudes in the low to mid stratosphere are shown in comparison to the Rawinsonde data. Also on this figure the data from the 1200Z, March 20 rawinsonde are included. The wind speed indicated by the IMAGER below 25 Km is consistently higher than the Rawinsonde data. It should be remembered that the calculated accuracy of the IMAGER is plus or minus 10 meters per second. Above 25 Km the IMAGER does a very good job of detecting the very light winds in this region. Notice, too, that the shape of the IMAGER profile follows well with the shape of the profile of the Rawinsonde data, including the small decrease in wind speed at around 17 Km. The possible reasons for the discrepancies in the wind measurements are discussed in the conclusions section of this paper.

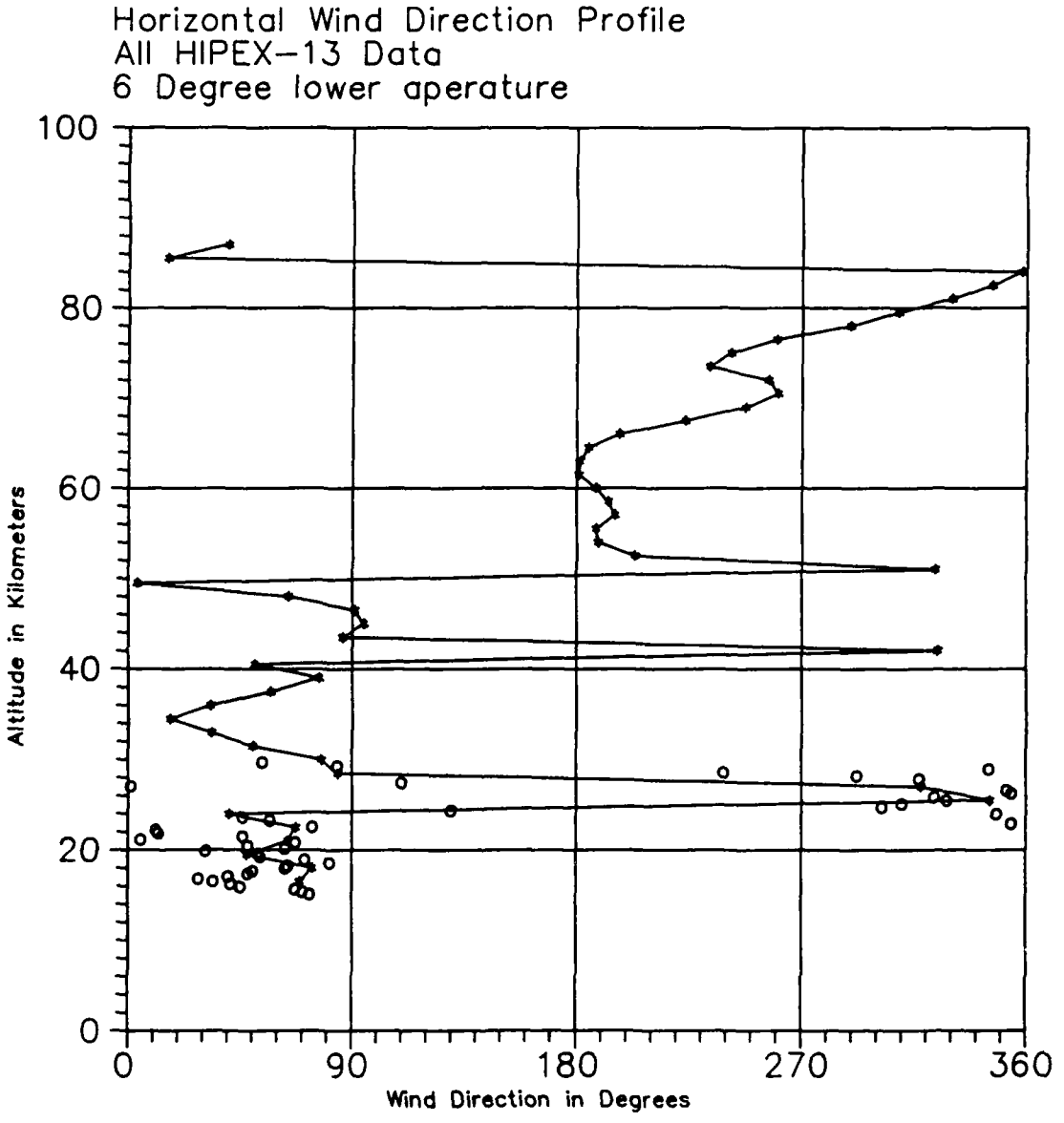

Fig. 12. A comparison of the horizontal wind direction of the IMAGER and Rawinsonde data.

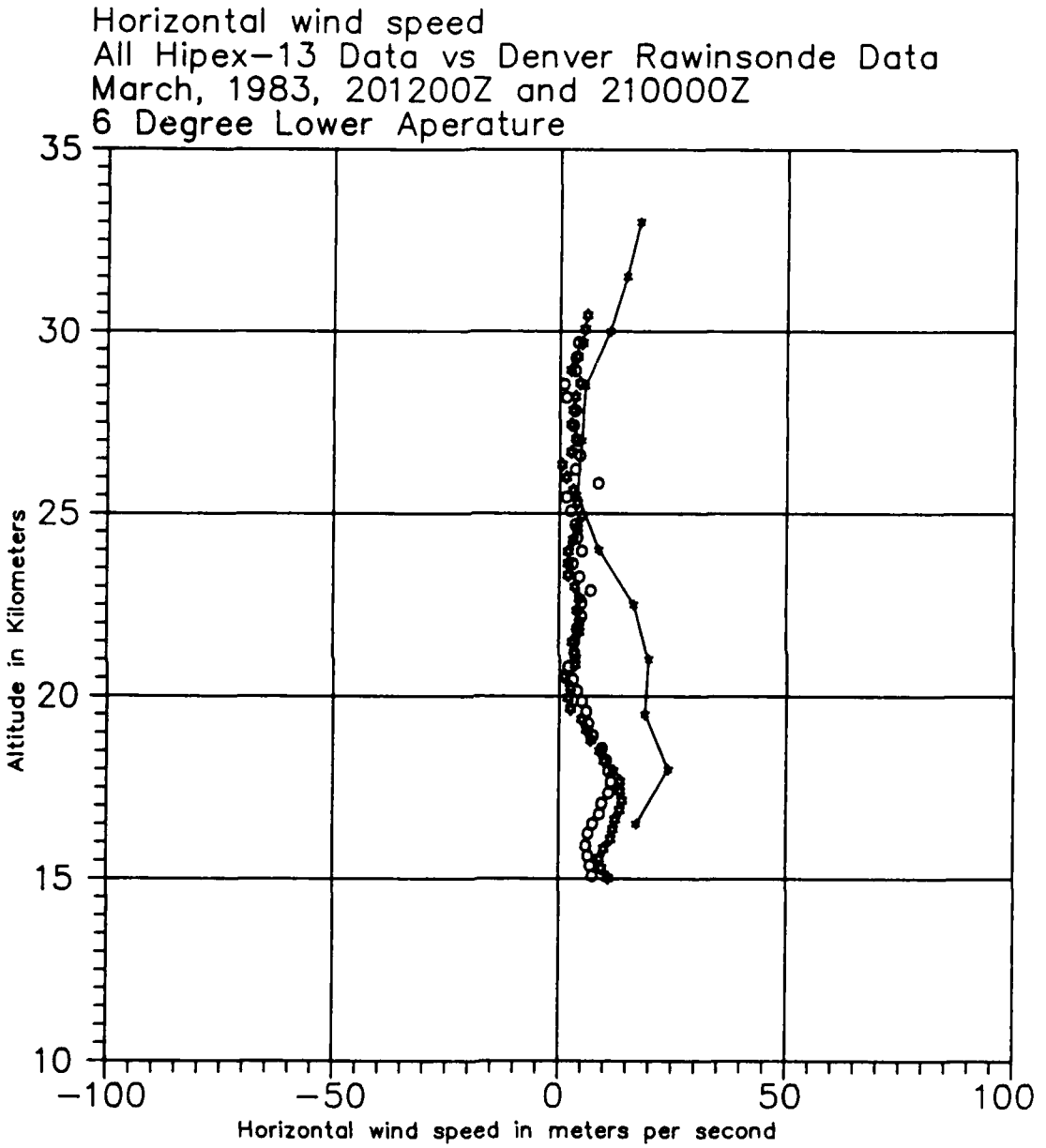

Fig. 13. A comparison of horizontal wind speed of the IMAGER and two Rawinsonde data runs, for the lower stratosphere.

Figure 14 illuminates the wind direction of the IMAGER data versus the two Rawinsonde runs. It should be taken into account that the indicated wind direction is not in the standard meteorological sense. That is, the direction of the wind is the direction in which the wind is travelling to, not from. This was taken into account when entering the Rawinsonde data. Above 25 Km there is a wide variability in direction in the Rawinsonde data, which is to be expected with the light and variable winds in this region. This can account for the discrepancies in the indicated wind directions of the IMAGER data with the Rawinsonde data.

Figure 15 shows a time series of the east-west wind component for all the data. This figure is taken from the data at 61.5 Km, which is the lowest altitude from which wind data can be obtained for each two minute file. Figures 16 - 18 show three consecutive altitudes and the variability in the east-west wind speeds of each. In the future, these data representations will be examined for wave motion that would be occurring. That is, an attempt will be made to find waves and their periods from these graphs, to include showing the possibility of waves propagating upward or downward.

Figure 19 is similar to the previous four figures except that it shows the time fluctuations of the vertical wind component for 61.5 Km. Figures 20 - 22 show profiles

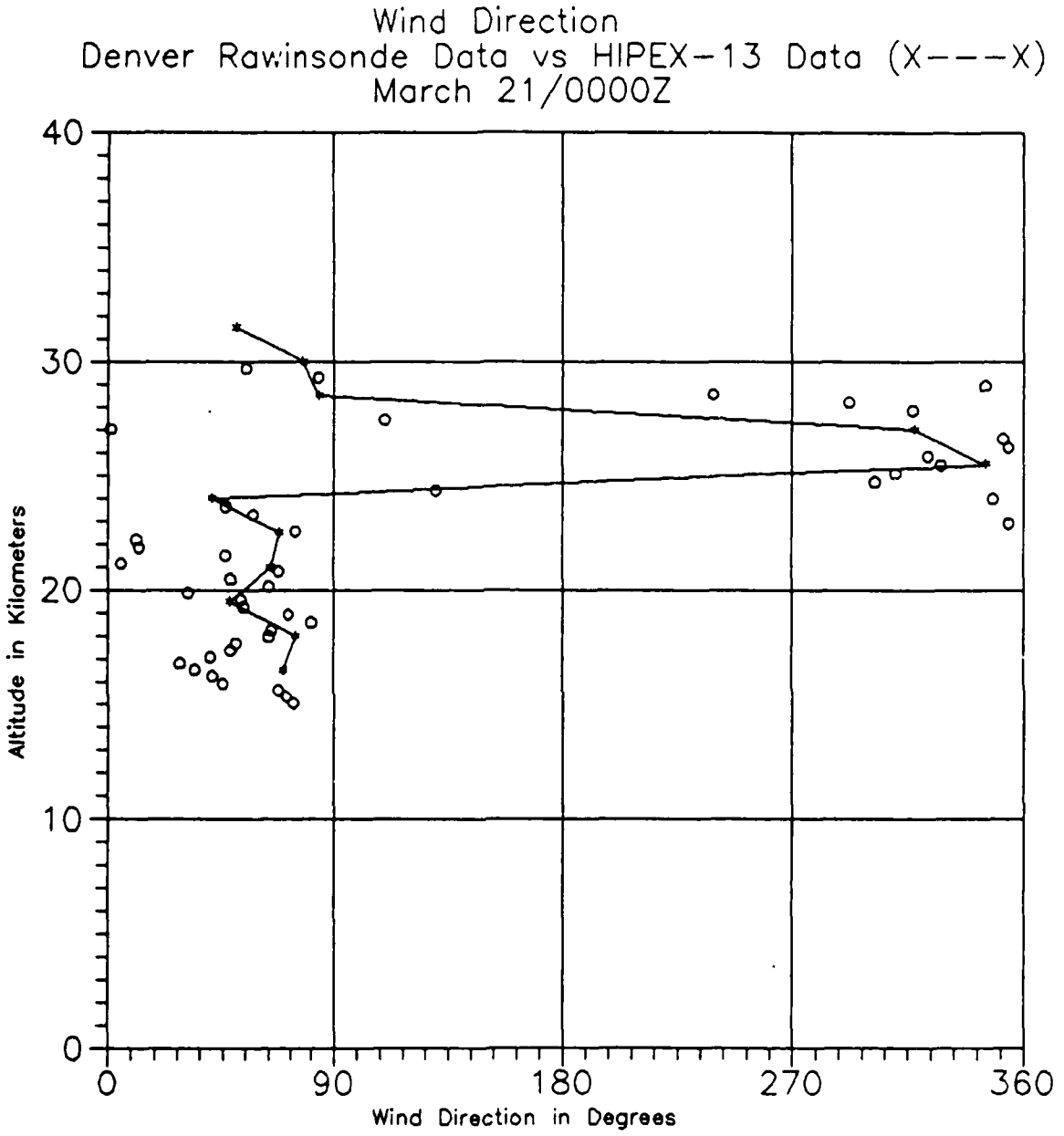

Fig. 14. A comparison of the horizontal wind direction of the IMAGER and a Rawinsonde data run, for the lower stratosphere.

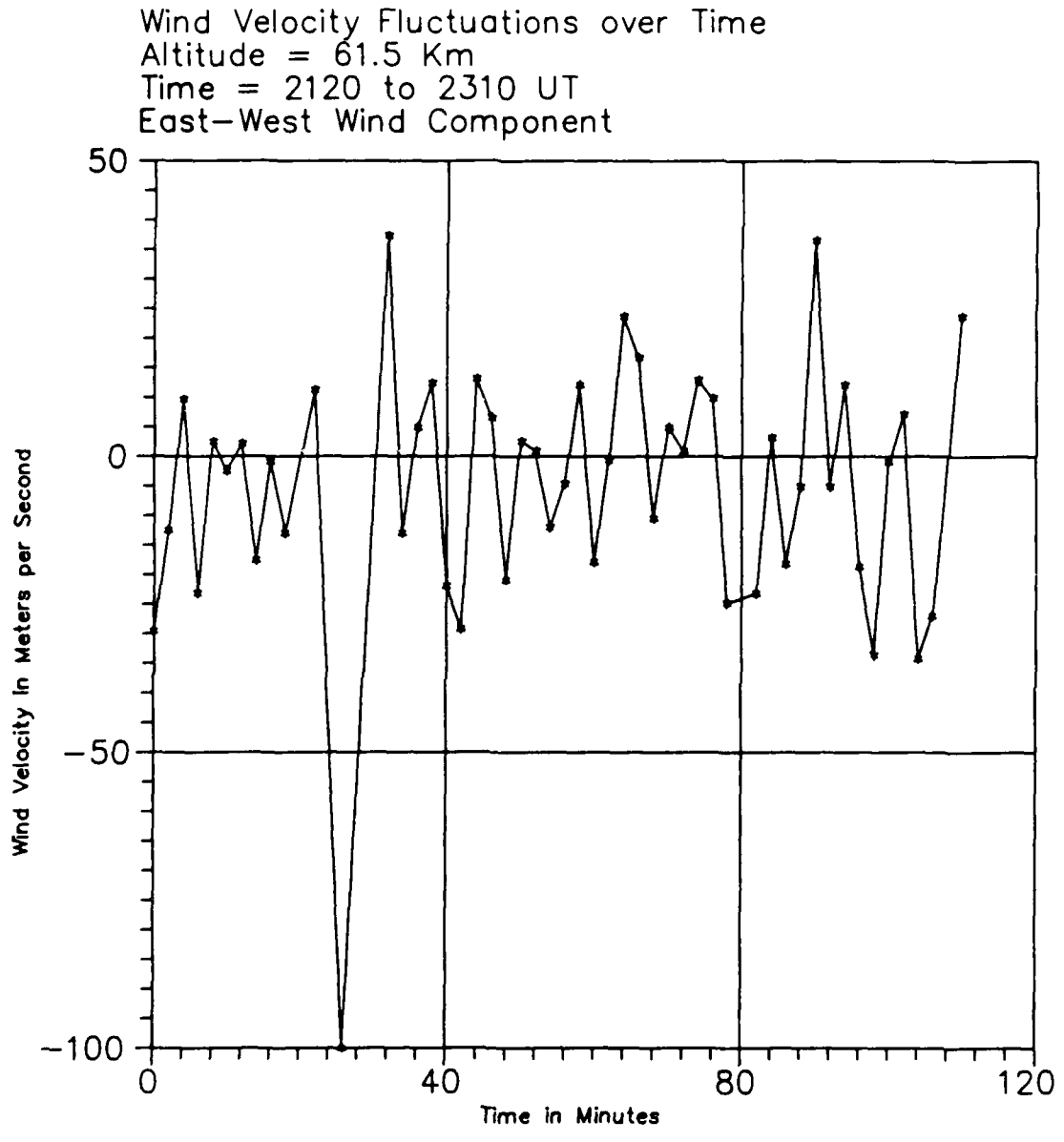

Fig. 15. East-West wind velocity fluctuations over time for 61.5 Km.

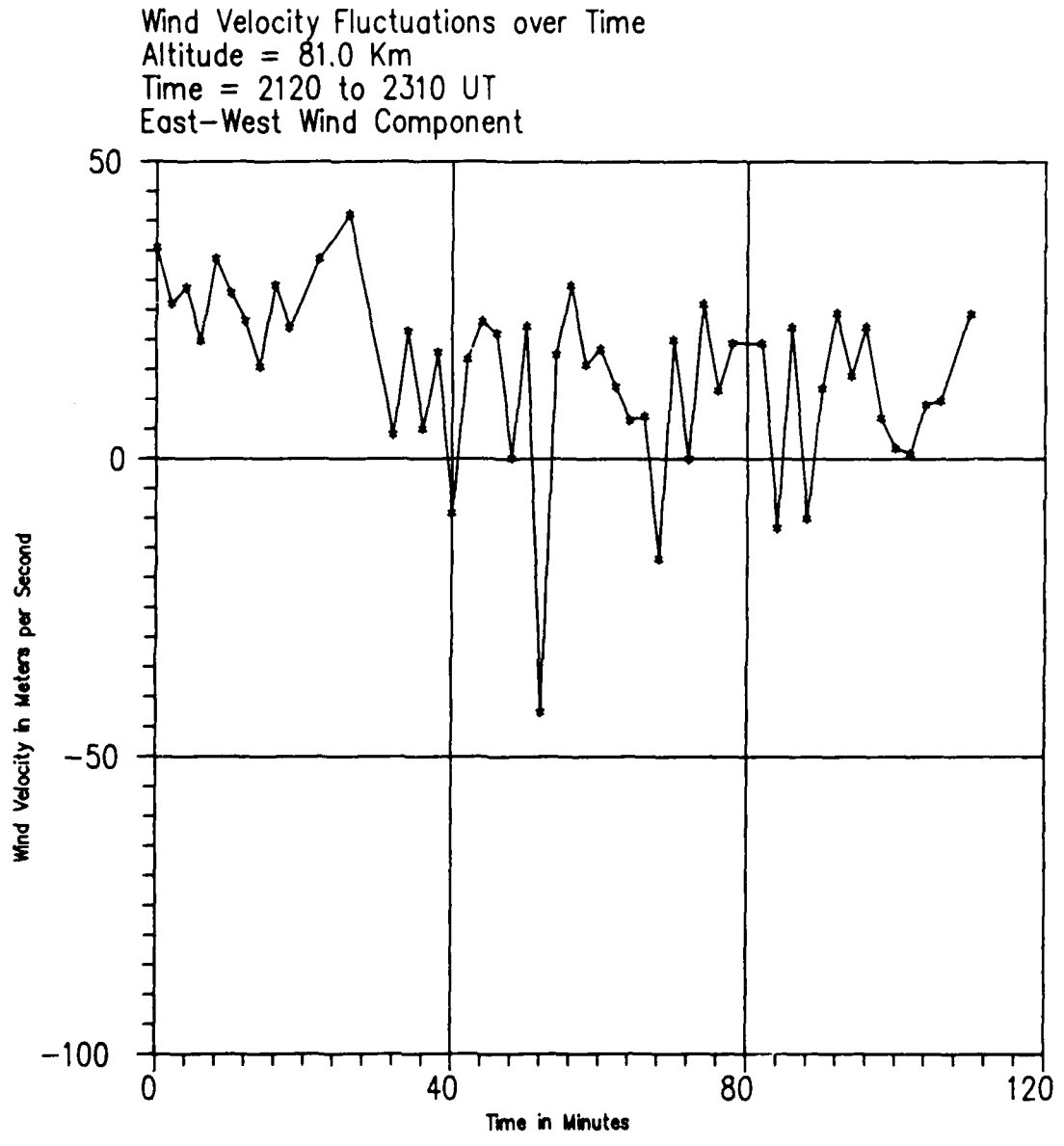

Fig. 16. East-West wind velocity fluctuations over time for 81.0 Km.

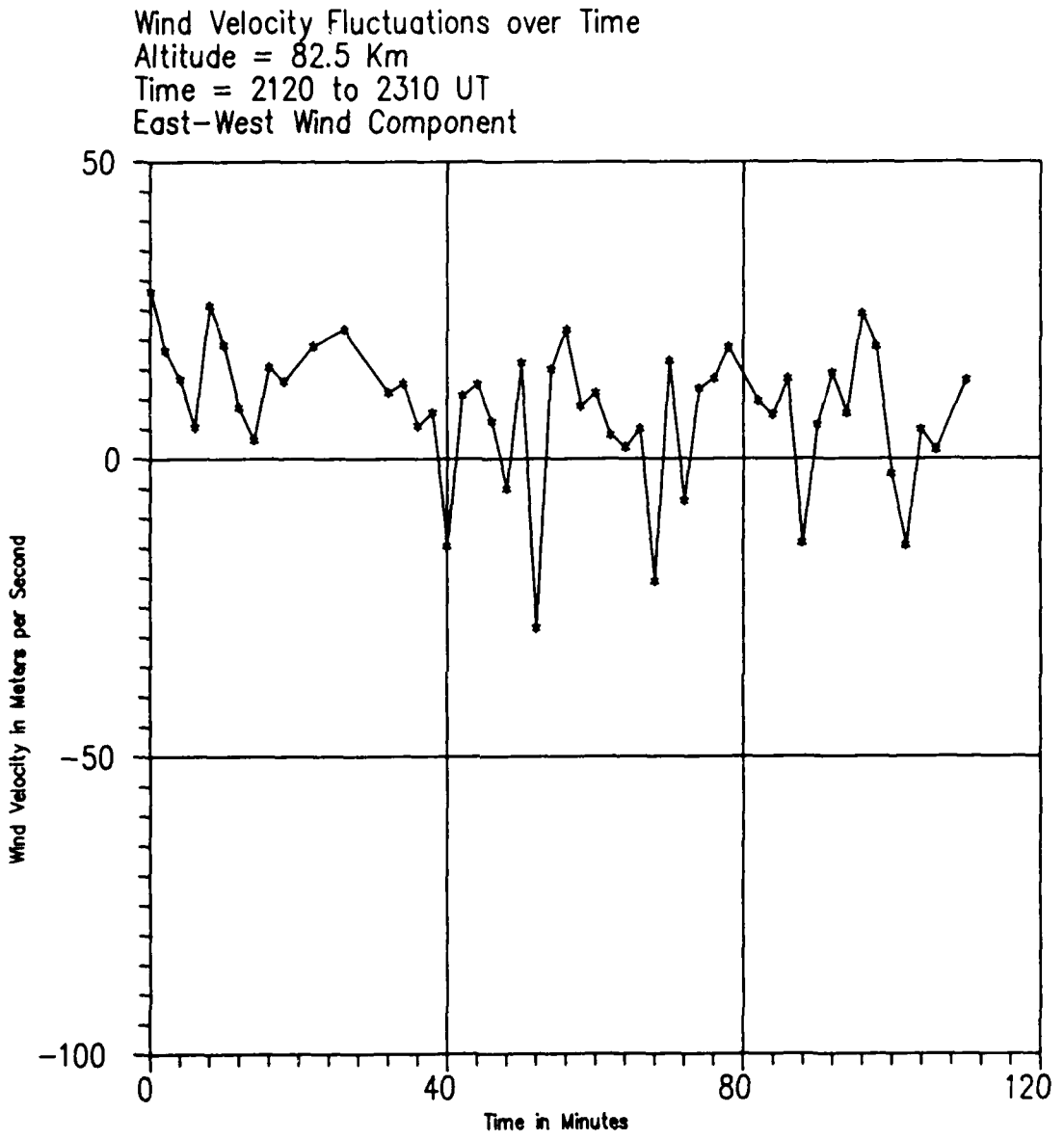

Fig. 17. East-West wind velocity fluctuations over time for 82.5 Km.

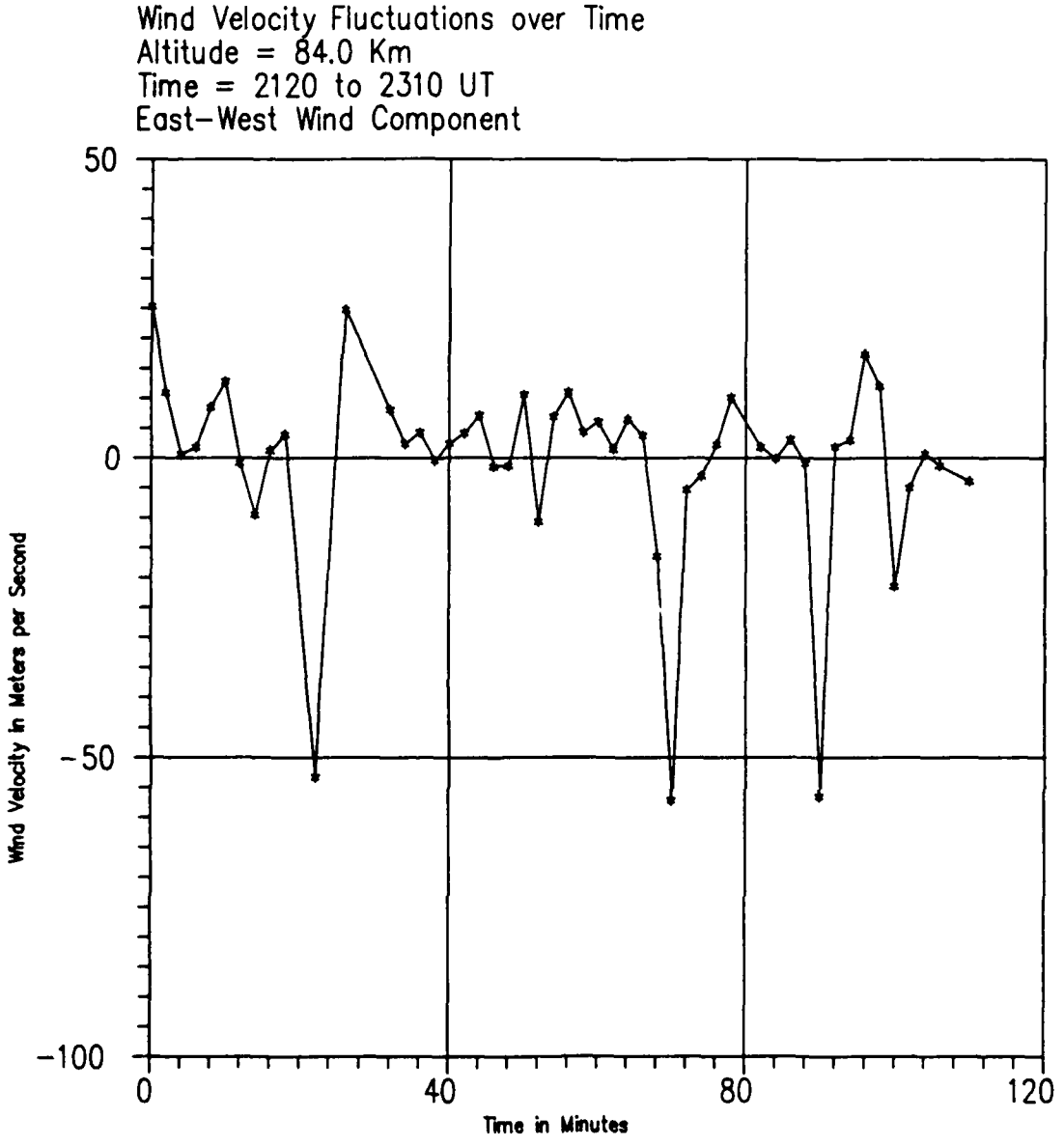

Fig. 18. East-West wind velocity fluctuations over time for 84.0 Km.

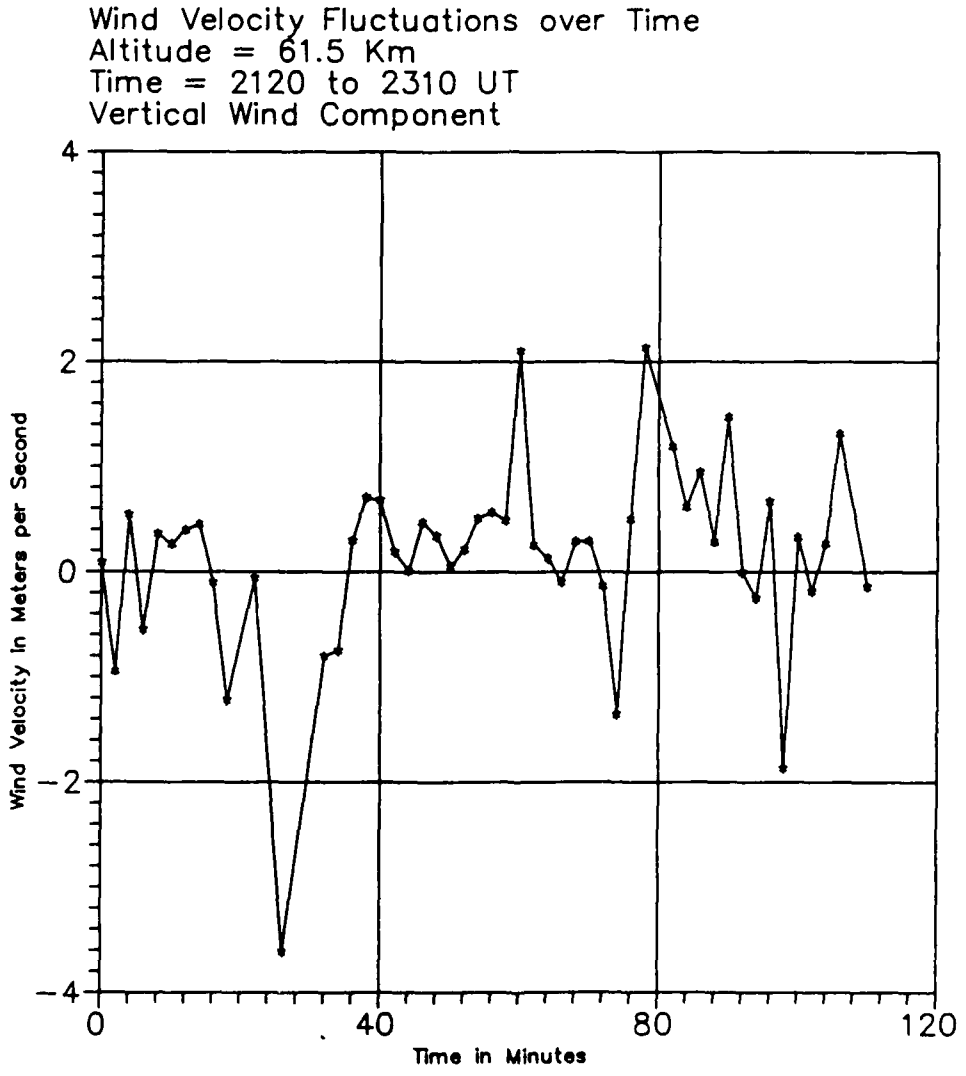

Fig. 19. Vertical wind velocity fluctuations over time for 61.5 Km.

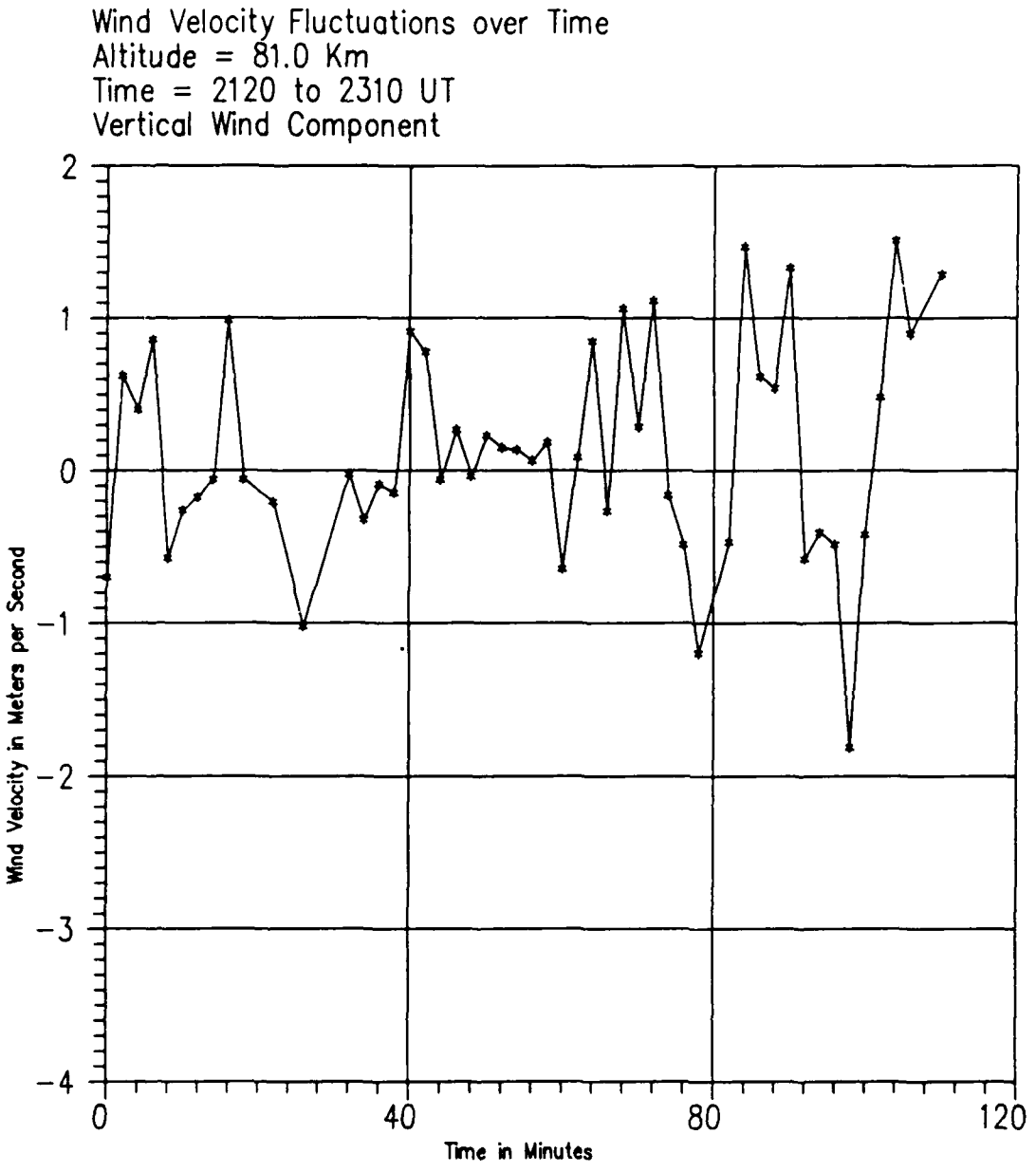

Fig. 20. Vertical wind velocity fluctuations over time for 81.0 Km.

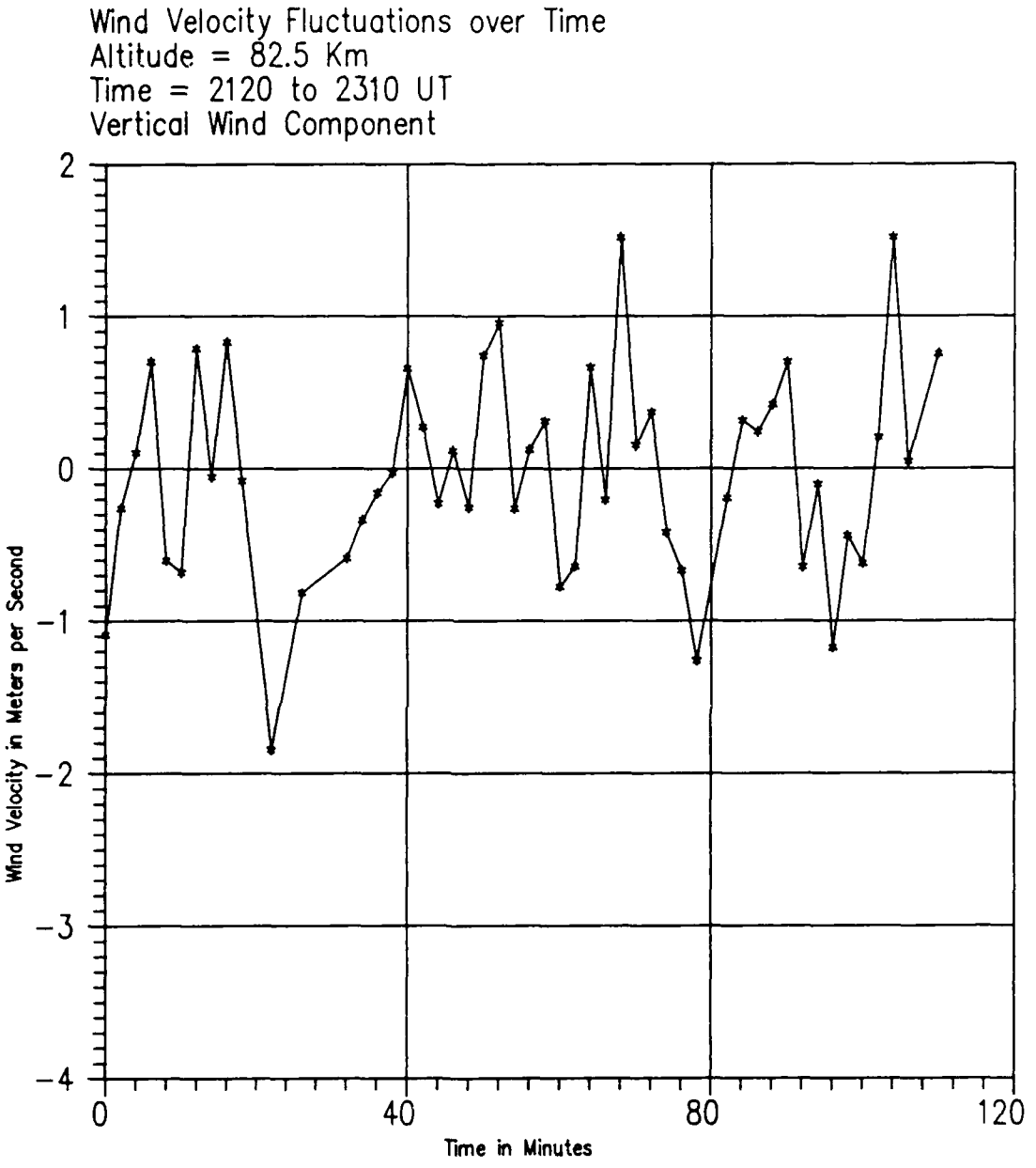

Fig. 21. Vertical wind velocity fluctuations over time for 82.5 Km.

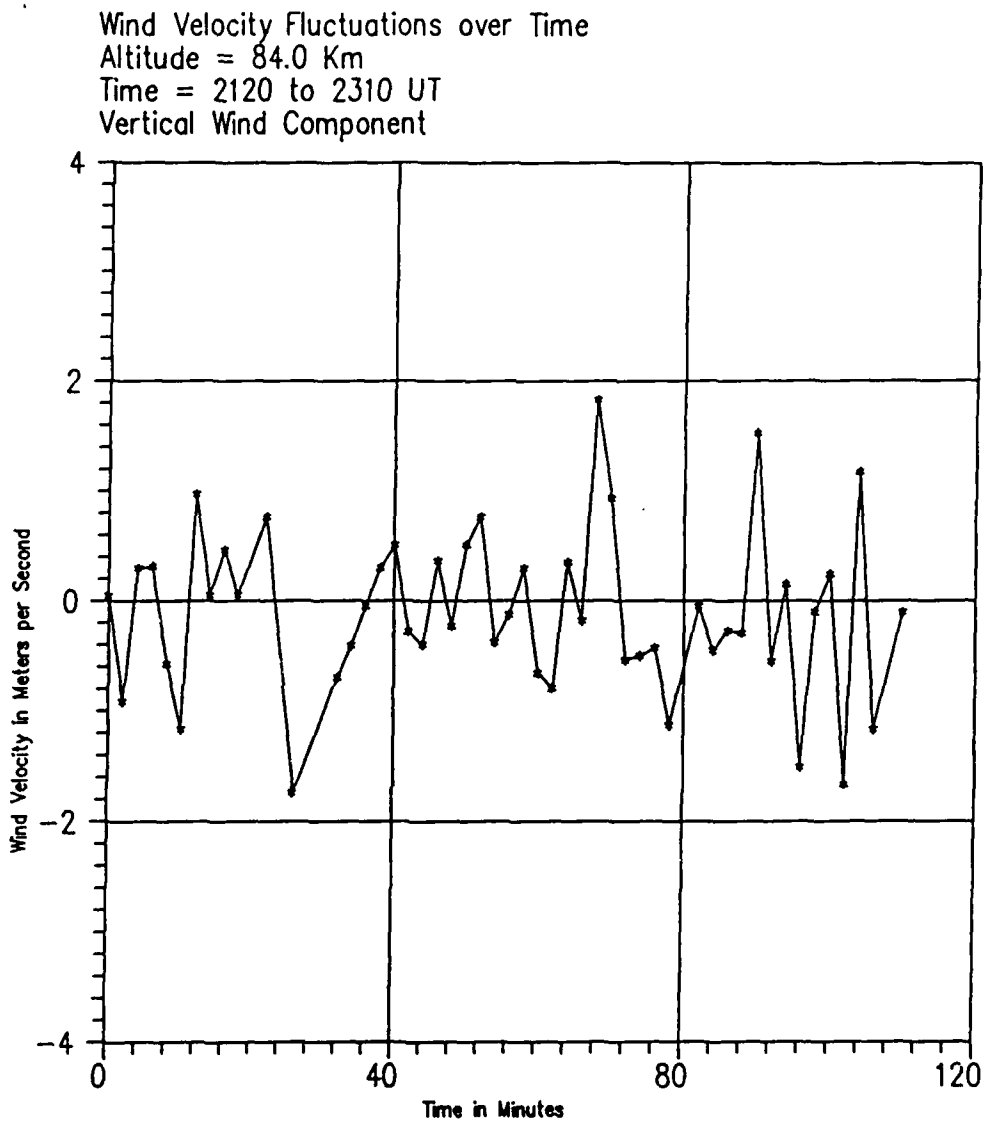

Fig. 22. Vertical wind velocity fluctuations over time for 84.0 Km.

for the same three altitudes as for the east-west wind. Once again, in the future these representations will be studied for wave patterns.

Figure 23 shows the vertical wind speed for the entire altitude range covered by the IMAGER. Notice that the wind speed indicated is less than plus or minus 1 meter per second. Compare this with the fluctuations in the speed observed in Figures 19 - 22. It appears that the speeds nearly average out over the entire time of data acquisition. That is, the wind starts with a speed directed downward but gradually shifts upward in the middle of the IMAGER data run. This should be further studied to see if this is just an anomaly in the data or is more indicative of what actually occurs.

Figure 24 shows the total power returned by those points used in the wind calculations. Notice how the power (in dB's) falls to a minimum near the stratopause at around 55 Km. This figure shows the sum of the power of all the points. Figure 25 shows the total number of points actually used in wind calculations versus the altitude. Again, this shows a dramatic increase in the number of points detected as the IMAGER looks at altitudes above 55 Km. Note, however, that the returns at the very bottom and very top (15 Km and 89 Km) should not be taken as valid. In other words, true data returns are in the range of 16.5 - 87.5 Km.

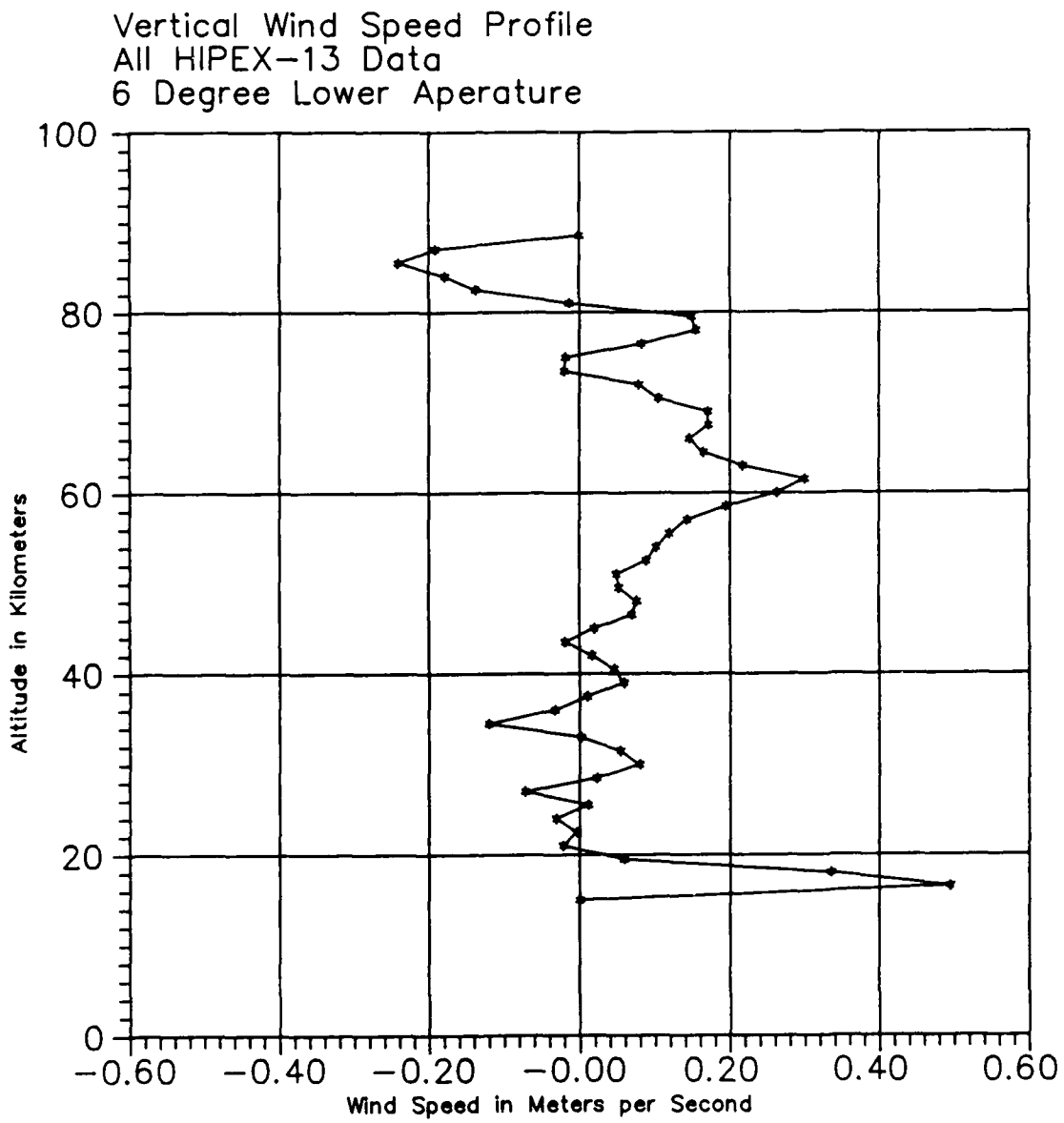

Fig. 23. Vertical wind speed profile for HIPEX-13.

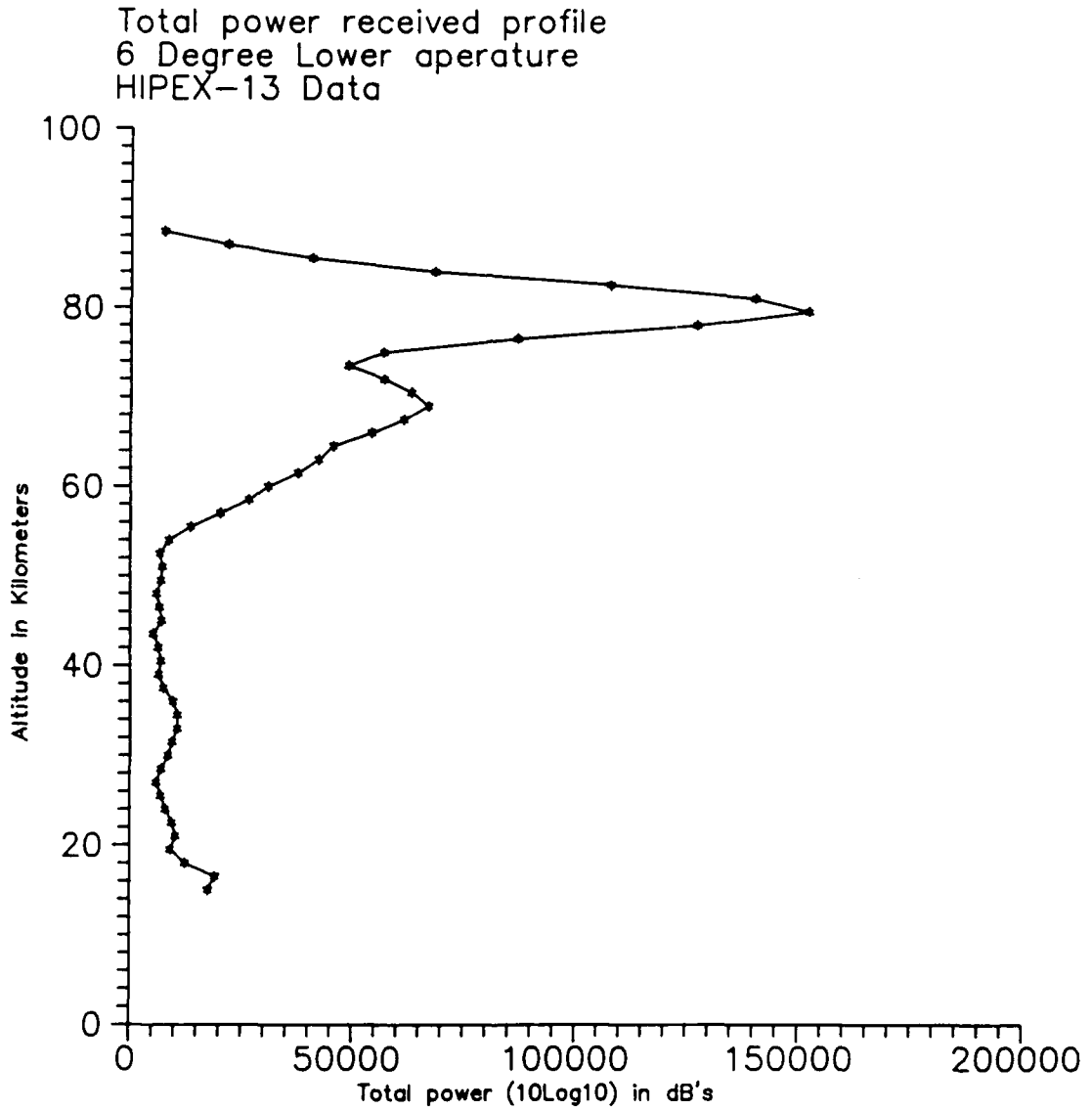

Fig. 24. Total power returned profile.

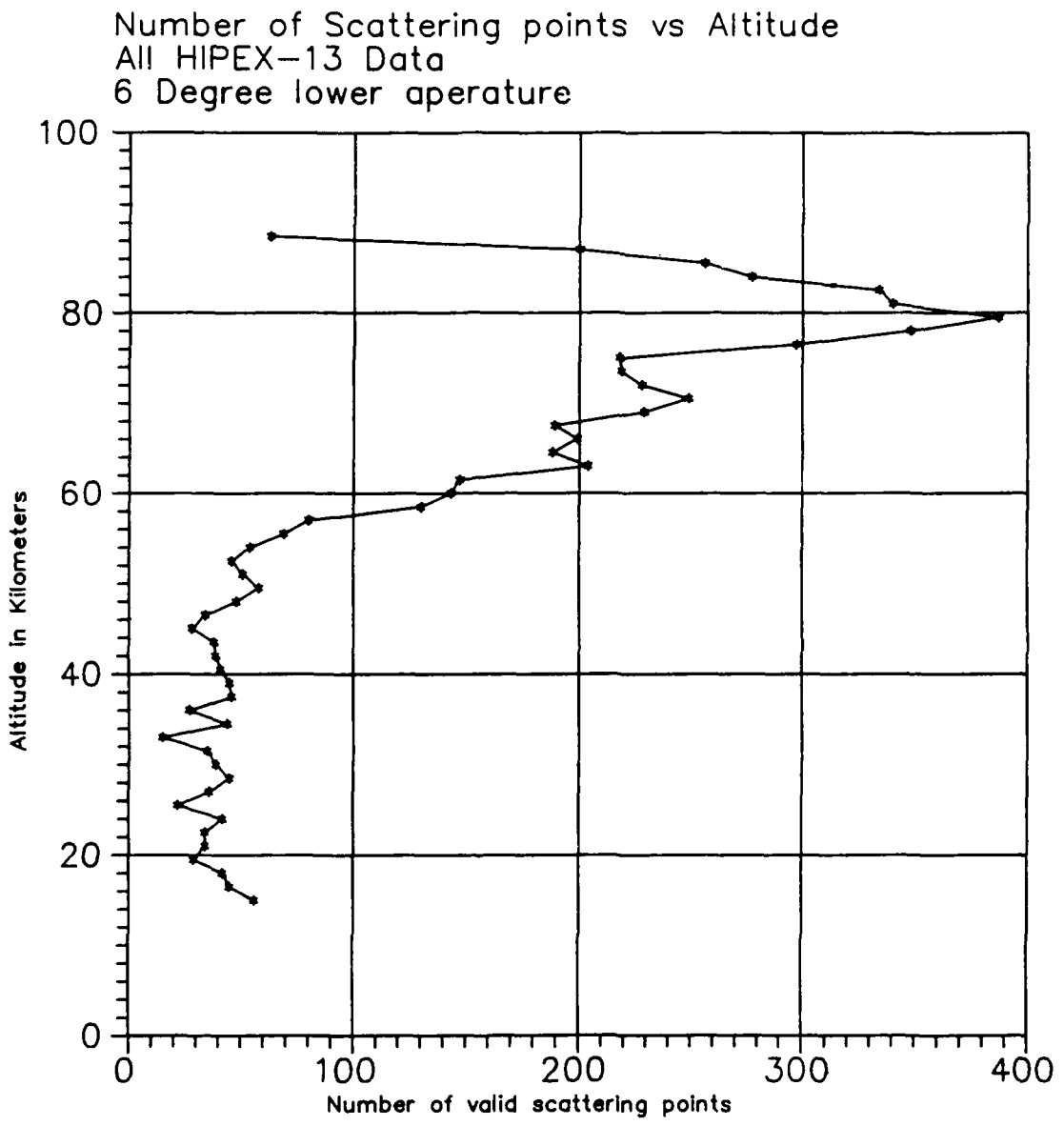

Fig. 25. Number of scattering points used in calculations profile.

Figure 26 is a closeup view of the altitude range covering the stratosphere with respect to total power returned. This better illustrates the sharp increase in power of the returns at the stratopause. As before, the bottom value for 15 Km is ambiguous and should not be considered as real.

Figure 27 is the tabulated rawinsonde data used in comparison with the IMAGER data. Note that the wind directions have been changed to reflect the direction the wind is heading to, which is the conventional way in the field of Aeronomy.

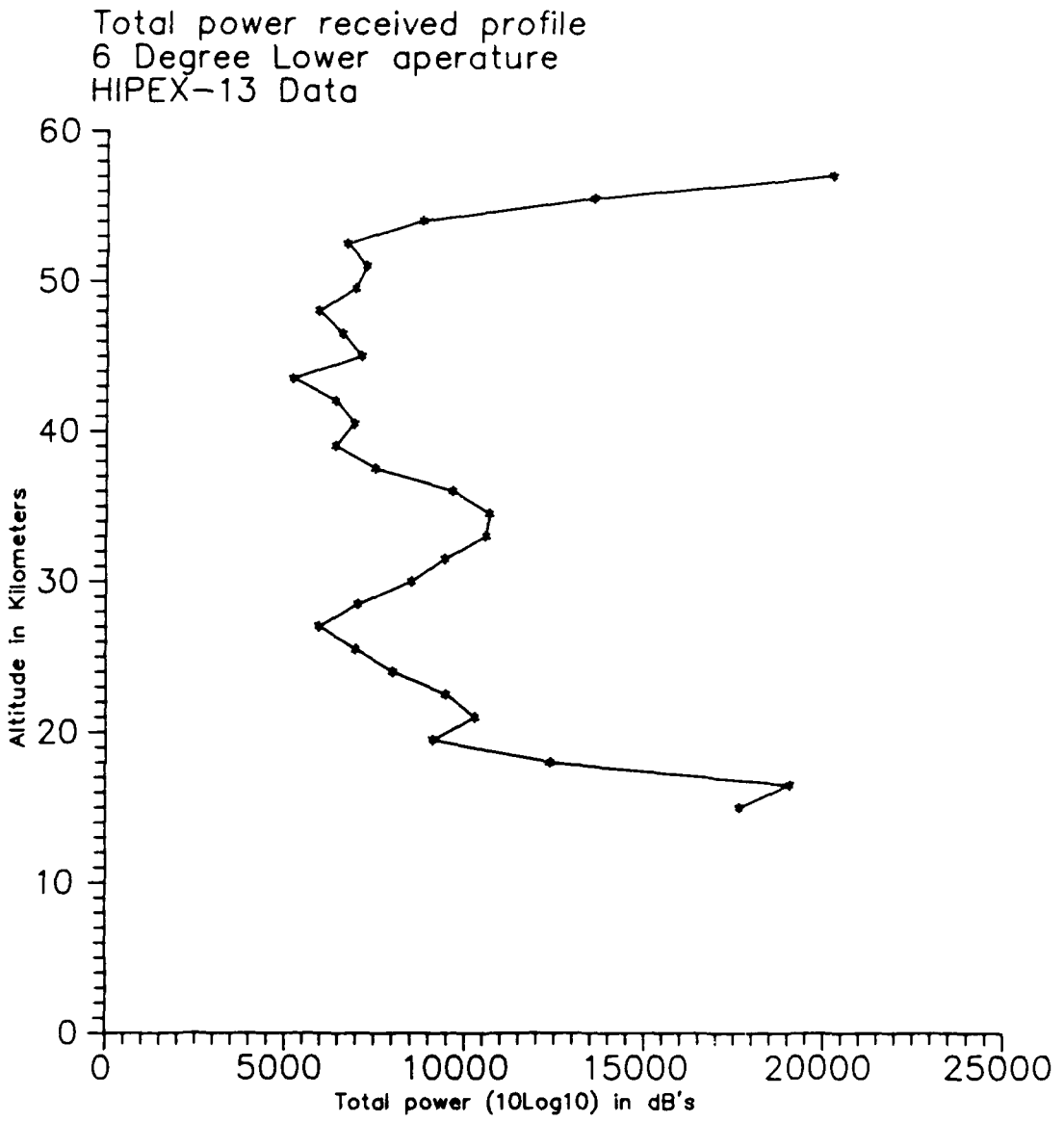

Fig. 26. Total power returned profile for the stratospheric range of altitudes.

Denver Rawinsonde Data
March 21/0000Z

Altitude (Km)	Speed (m/s)	Direction (degrees)
15.08	7.5	73
15.36	7.0	69
15.63	6.5	67
15.91	6.0	45
16.24	6.5	41
16.51	7.5	34
16.78	9.0	28
17.07	9.5	40
17.36	11.0	48
17.66	11.5	50
17.95	11.0	63
18.24	10.5	64
18.57	9.5	81
18.92	7.5	71
19.25	6.5	53
19.58	6.0	52
19.86	5.0	31
20.14	4.0	63
20.45	3.0	48
20.80	2.0	67
21.14	3.5	5
21.49	3.5	46
21.84	4.0	12
22.18	5.0	11
22.54	5.0	74
22.89	7.0	354
23.26	4.5	57
23.62	3.0	46
23.97	5.0	348
24.33	4.0	130
24.69	3.5	302
25.07	2.5	310
25.45	1.5	328
25.83	8.5	323
26.21	3.5	354
26.59	4.5	352
27.01	4.0	1
27.42	3.0	110
27.83	3.5	317
28.19	1.5	292
28.55	1.0	239
28.92	3.5	345
29.28	3.5	84
29.69	4.0	54

Fig. 27. March 21/0000Z rawinsonde data of height vs wind speed and wind direction.

CHAPTER V

CONCLUSIONS AND RECOMMENDATIONS

The results shown indicate that the IMAGER does provide winds in the critical region of the middle atmosphere between 30 and 60 Km. This would be a first for a radar, and this fact makes this radar an important tool for further studies of this region of the atmosphere.

The following specific conclusions can be made:

1) The IMAGER is capable of providing wind speed and direction for the entire altitude range of the middle atmosphere (20 - 90 Km). By trial and error, it was determined that a minimum of three data files of two minutes each are needed to provide a complete profile, although occasionally one file may have enough scattering points to provide a complete profile. It has been again demonstrated that the IMAGER can provide wind measurements above 60 Km with just one two minute file of data.

2. The IMAGER winds compare favorably to an order of magnitude with the winds indicated by the Rawinsonde data taken from Denver for a time only a few hours before and after the IMAGER data collection period. Any discrepancies between the two data sets can be attributed to the decreased accuracy of the IMAGER in

comparison with a Rawinsonde balloon. Also, in the altitudes between 20 and 30 Km the low wind velocities as observed by the rawinsonde vary greatly with the IMAGER data due to the poor resolution of the IMAGER. This resolution can be improved, and these preliminary results indicate that the winds from these two measurement techniques may ultimately agree. Overall, the general shape of the profile from the IMAGER compares well with the shape of the Rawinsonde data.

With these results, several possible applications of the IMAGER come to mind. First of all, one should be aware that the IMAGER was developed and installed in 1983. Since then there have been advances in the accuracy of the hardware which the IMAGER used to collect and analyze the data. In addition, there are probably better transformation routines that have been developed than the one used here, the IMSL routine for Fourier transformation. Longer files with regards to the number of scattering points would enhance the results of the Fourier transformation by providing a longer period of record for the transformation.

A vast improvement over the original IMAGER would be to install the hardware and software used to derive the winds at the radar site. That is, as the data are acquired by the IMAGER, winds could be derived right on the spot, thus providing "real time" wind calculations. That would

be the ultimate goal of a radar providing wind information: to provide instantaneous wind readings.

Why would anyone care to know what the winds are doing in the middle atmosphere? It has become apparent in recent years that Man is becoming more concerned with this region as one with great potential. With the coming development of the hypersonic and hypervelocity aircraft (the Orient Express, for example) the need to know the wind conditions in the middle atmosphere becomes quite apparent. Also, this is a region in which all space vehicles must ascend through on their way into orbit. The knowledge of a possible sheer condition at a high altitude may be of importance to such a vehicle. Also, the recent push concerning the Strategic Defense Initiative ("Star Wars") must take into account wind velocities and directions as a defensive system against ballistic missiles is developed.

LITERATURE CITED

Adams, G. W., J. W. Brosnahan, D. C. Walden, and S. F. Nerney, 1986: Mesospheric observations using a 2.66-MHz radar as an Imaging Doppler Interferometer: Description and First Results. Journal of Geophysical Research, 91, 1671-1683.

——, D. P. Edwards, and J. W. Brosnahan, 1985: The Imaging Doppler Interferometer: Data analysis. Radio Science, 20, No. 6, 1481-1492.

Balsley, B. B. and K. S. Gage, 1980: The MST radar technique: Potential for middle atmospheric studies. Pageoph, 118, 452-493.

——, and ——, 1981: On the vertical-incidence VHF backscattered power profile from the stratosphere. Geophysical Research Letters, 8, No. 11, 1173-1175.

Farley, D. T., 1983: Radar Interferometer Measurements. Handbook for MAP, 9, SCOSTEP Secretariat, University of Illinois, Urbana, Illinois, 237-240.

Gage, K. S., and T. E. VanZandt, 1981: Wind measurement techniques available for the middle atmosphere program. Journal of Geophysical Research, 86 (C 10), 9591-9598.

Johnson, R.E., G. W. Adams, and J. W. Brosnahan, 1986: Specularity measurements of the middle atmosphere using an Imaging radar. Presented at the 1986 AGU Fall Meeting, San Francisco, December 8-12, 1986.

Larsen, M. F., 1983: The MST radar technique: A tool for investigations of tuburbulent spectra, MAP Handbook, 9, SCOSTEP Secretariat, University of Illinois, Urbana, Illinois, 250-255.

Rottger, J., 1980: Structure and dynamics of the stratosphere and mesosphere revealed by VHF radar investigations. Pageoph, 118, 494-527.

Rottger, J., 1981: Investigations of lower and middle atmosphere dynamics with spaced antenna drifts radars. Journal of Atmospheric and Terrestrial Physics, 43, No. 4, 277-292.

Royrvik, O., 1983: Implication on data interpretation by short- and long-period oscillations. MAP Handbook, 9, SCOSTEP Secretariat, University of Illinois, Urbana, Illinois, 228-231.

——, 1984: Morphology of the scattering targets: Fresnel and turbulent mechanisms. Notes from the Second Workshop on the Technical Aspects of MST Radar, SCOSTEP Secretariat, University of Illinois, Urbana, Illinois, May 21-25, 1984.

Stubbs, T. J., 1973: The measurement of winds in the D-region of the ionosphere by the use of partially reflected radio waves. Journal of Atmospheric and Terrestrial Physics, 35, 909-919.

Tsuda, T., T. Sato, K. Hirose, S. Fukao, and S. Kato, 1986: MU radar observations of the aspect sensitivity of backscattered VHF echo power in the troposphere and lower stratosphere. Radio Science, 21, No. 6, 971-980.

Vincent, R. A., 1984: Topic 3. Relationship of spaced antenna and Doppler techniques for velocity measurements (Keynote paper). Notes from the Second Work-Shop on Technical Aspects of MST Radar, SCOSTEP Secretariat, University of Illinois, Urbana, Illinois, May 21-25, 1984.

Warnock, J. M., T. E. VanZandt, J. L. Green, and R. H. Winkler, February, 1978: Comparison between wind profiles measured by Doppler radar and by Rawinsonde balloons. Geophysical Research Letters, 5, No. 2, 109-112.

Woodman, R. F., 1971: Inclination of the geomagnetic field measured by an incoherent scatter technique. Journal of Geophysical Research, 31, 178-184.

END

12-87

DTIC